ATLAS検出器と物理入門（その2）
内部飛跡検出器

	9:30-10:30	10:30-12:30		午後
8月1日（木）	開校式	山村(1)「LHCにおけるATLAS実験」高エネルギーニュース Vol.15 No.1, p16-27, April 1996		
8月2日（金）	検出器1 序論 (C.Joram@CERN夏の学校，田中礼)	山村(2)		
8月3日（土）	ICHEP2002報告（岩崎博行先生）トラペ	皆川(1) Higgs→γγ (TDR P.675-684)		CompHEP講座 実技入門編（浅井）
8月4日（日）	休み（だったハズだが仕事した）			
	9:15-10:00	10:15-11:15	11:15-12:30	
8月5日（月）	LHCでの物理1 (F.Gianotti)	検出器2 飛跡検出器（岩田洋世先生）		CMS見学（久里先生）写真
8月6日（火）	LHCでの物理2 (F.Gianotti)	検出器2 飛跡検出器（岩田洋世先生）	皆川(2)	
8月7日（水）	LHCでの物理3 (F.Gianotti)	検出器3 シンチレーション、光検出器（田中礼）	皆川(3)	COMPASS見学（岩田高広先生）写真

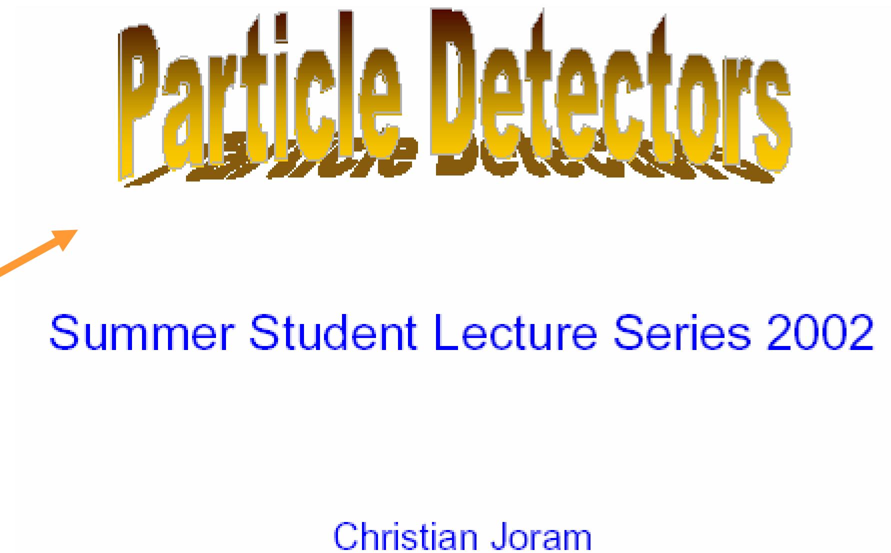

http://www.icepp.s.u-tokyo.ac.jp/~asai/higgs-work/curriculum_2002.html

KEK 池上

ATLAS Inner Detector

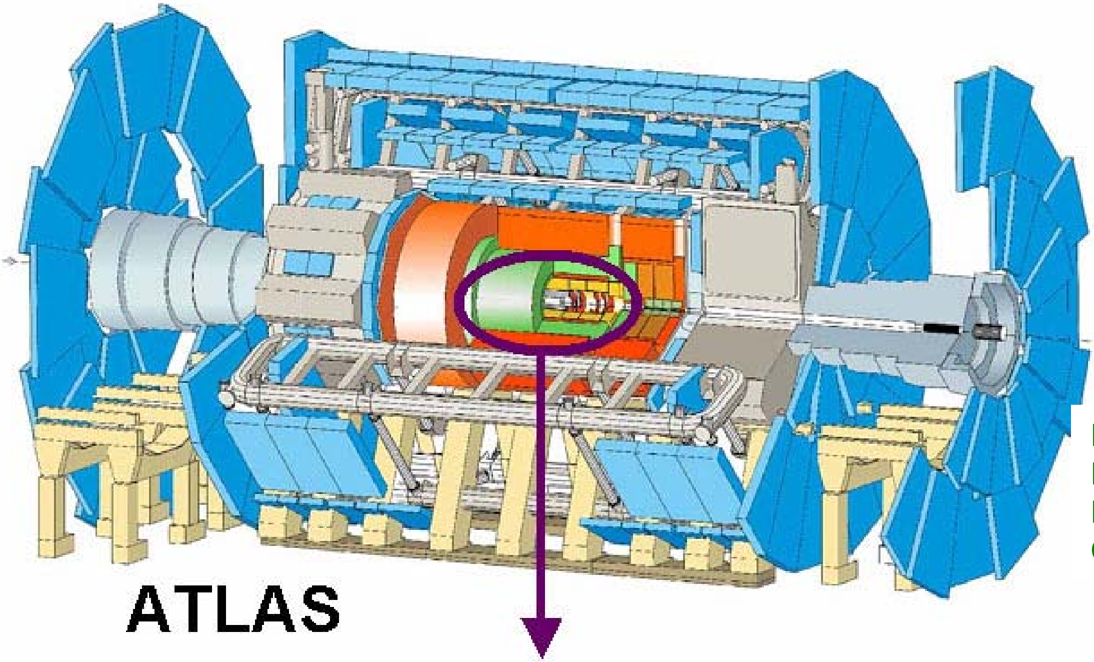

Diameter	25 m
Barrel toroid length	26 m
End-cap end-wall chamber span	46 m
Overall weight	7000 Tons

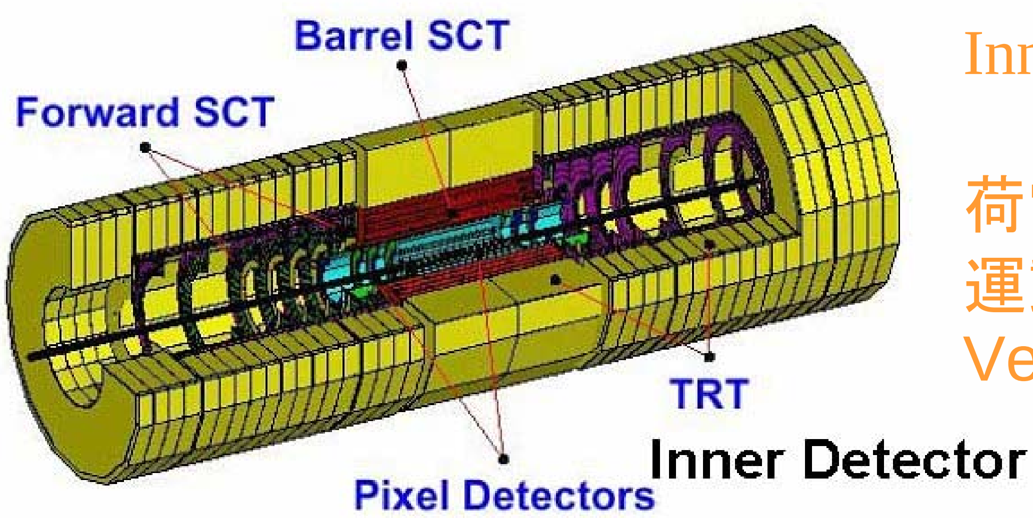

Inner detector + solenoid

↓

荷電粒子(e, μ , π)

運動量の測定

Vertex pointの測定

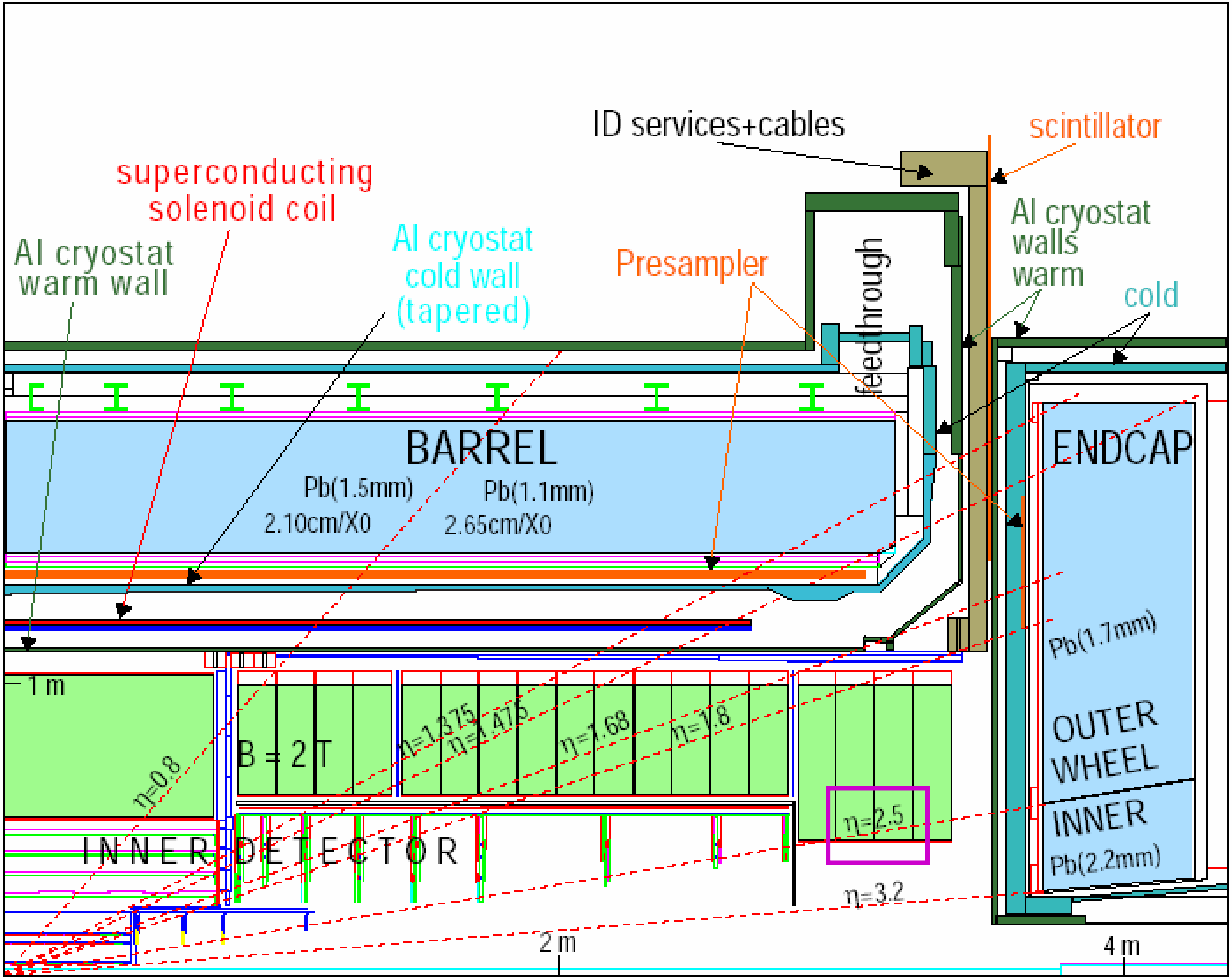

Figure 4-i Longitudinal view of a quadrant of the ATLAS EM Calorimeter.

Momentum measurement

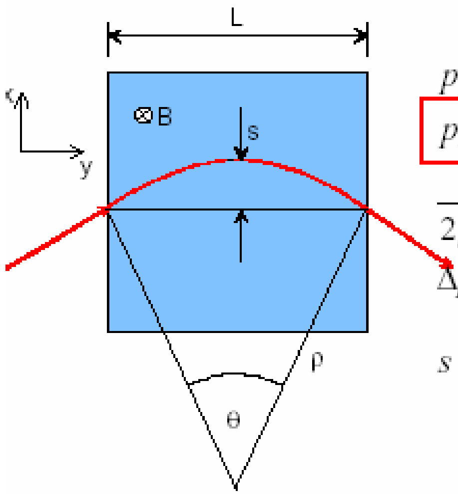

$$p_T = qB\rho$$

$$p_T\,(\mathrm{GeV/c}) = 0.3B\rho \quad (\mathrm{T\cdot m})$$

$$\frac{L}{2\rho} = \sin\theta/2 \approx \theta/2 \quad\rightarrow\quad \theta \approx \frac{0.3L\cdot B}{p_T}$$

$$\Delta p_T = p_T \sin\theta \approx 0.3L\cdot B$$

$$s = \rho(1-\cos\theta/2) \approx \rho\frac{\theta^2}{8} \approx \frac{0.3}{8}\frac{L^2 B}{p_T}$$

$\sigma(1/pt) \propto \sigma x$

the sagitta s is determined by 3 measurements with error $\sigma(x)$: $s = x_2 - \frac{x_1 + x_3}{2}$

$$\left.\frac{\sigma(p_T)}{p_T}\right|^{meas.} = \frac{\sigma(s)}{s} = \frac{\sqrt{\frac{3}{2}}\sigma(x)}{s} = \frac{\sqrt{\frac{3}{2}}\sigma(x)\cdot 8\,p_T}{0.3\cdot BL^2}$$

for N equidistant measurements, one obtains

(R.L. Gluckstern, NIM 24 (1963) 381)

$$\left.\frac{\sigma(p_T)}{p_T}\right|^{meas.} = \frac{\sigma(x)\cdot p_T}{0.3\cdot BL^2}\sqrt{720/(N+4)} \qquad \text{(for } N \geq \approx 10\text{)}$$

ex: p_T=1 GeV/c, L=1m, B=1T, $\sigma(x)$=200μm, N=10

$$\left.\frac{\sigma(p_T)}{p_T}\right|^{meas.} \approx 0.5\% \qquad (s \approx 3.75\ \mathrm{cm})$$

ATLASの近似として、

Pt =500 GeV/c

L =1 m

B =2 T

σx=60 μm

N =50

→ 20 %

Scattering

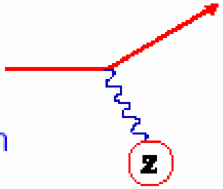

An incoming particle with charge z interacts with a target of nuclear charge Z. The cross-section for this e.m. process is

$$\frac{d\sigma}{d\Omega} = 4zZr_e^2\left(\frac{m_e c}{\beta p}\right)^2 \frac{1}{\sin^4\theta/2}$$

Rutherford formula

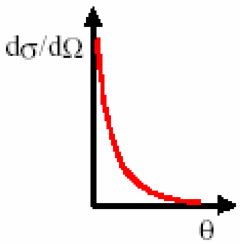

- Average scattering angle $\langle\theta\rangle = 0$
- Cross-section for $\theta \to 0$ infnite !

Multiple Scattering

Sufficiently thick material layer

→ the particle will undergo multiple scattering.

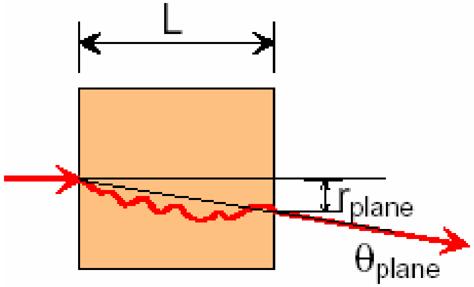

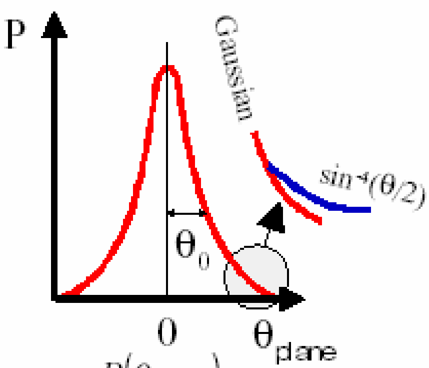

$$\theta_0 = \theta_{plane}^{RMS} = \sqrt{\langle \theta_{plane}{}^2 \rangle} = \frac{1}{\sqrt{2}}\theta_{space}^{RMS}$$

$$P(\theta_{plane}) = \frac{1}{\sqrt{2\pi}\,\theta_0}\exp\left\{-\frac{\theta_{plane}{}^2}{2\theta_0^2}\right\}$$

Approximation $\theta_0 = \frac{13.6\,MeV}{\beta c p} z \sqrt{\frac{L}{X_0}} \left\{ 1 + 0.038 \ln\left(\frac{L}{X_0}\right) \right\}$

X_0 is radiation length of the medium (discuss later)

(accuracy ≤ 11% for $10^{-3} < L/X_0 < 100$)

Back to momentum measurements:

contribution from multiple scattering

$$\Delta p^{MS} = p \sin\theta_0 \approx p \cdot 0.0136 \frac{1}{p} \sqrt{\frac{L}{X_0}}$$

$$\left.\frac{\sigma(p)}{p_T}\right|^{MS} = \frac{\Delta p^{MS}}{\Delta p_T} = \frac{0.0136\sqrt{\frac{L}{X_0}}}{0.3BL} = 0.045 \frac{1}{B\sqrt{LX_0}}$$

independent of p !

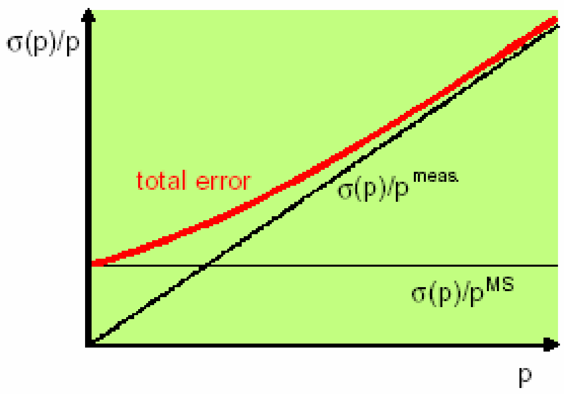

ex: Ar (X_0=110m), L=1m, B=1T $\left.\frac{\sigma(p)}{p_T}\right|^{MS} \approx 0.5\%$

ATLASの近似として、

L =1 m

B =2 T

L/X0=0.5

→ 2%

Momentum measurement in experiments with solenoid magnet:

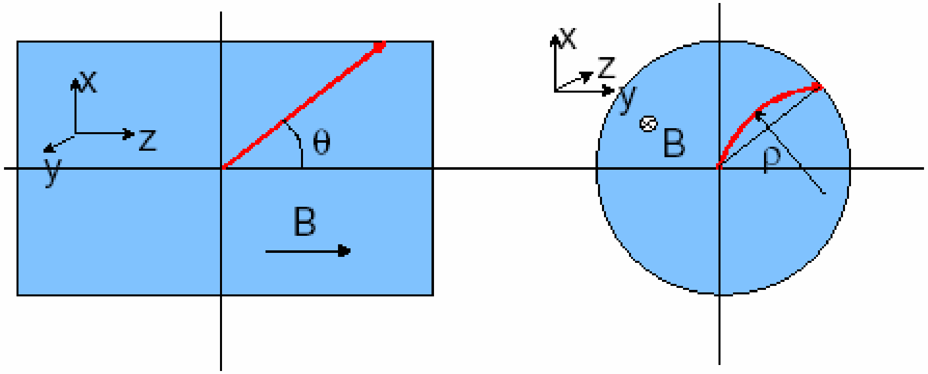

$p_T = p \sin\theta$

polar angle has to be determined from a straight line fit x=x(z).

N equidistant points with error $\sigma(z)$

$$\sigma(\theta)\Big|^{meas.} = \frac{\sigma(z)}{L}\sqrt{12(N-1)/(N(N+1))}$$

\+ multiple scattering contribution…. } normally small

In practical cases: $\frac{\sigma(p)}{p} \approx \frac{\sigma(p_T)}{p_T}$

In summary: $$\frac{\sigma(p)}{p}\Bigg|^{meas.} \propto \frac{\sigma(x)\cdot p}{BL^2}\frac{1}{\sqrt{N}}$$

Detection of charged particles

How do they loose energy in matter ?

- Discrete collisions with the atomic electrons of the absorber material.

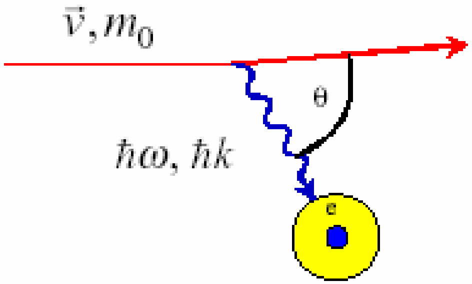

$$\left\langle \frac{dE}{dx} \right\rangle = -\int_0^\infty NE \frac{d\sigma}{dE} \hbar \, d\omega$$

N : electron density

Collisions with nuclei not important ($m_e << m_N$).

- If $\hbar\omega, \hbar k$ are big enough ⇨ ionization.

Instead of ionizing an atom, under certain conditions the photon can also escape from the medium.

⇨ Emission of **Cherenkov** and **Transition** radiation. (See later).

Average differential energy loss $\left\langle \frac{dE}{dx} \right\rangle$

Ionisation only → Bethe - Bloch formula

$$\left\langle \frac{dE}{dx} \right\rangle = -4\pi N_A r_e^2 m_e c^2 z^2 \frac{Z}{A} \frac{1}{\beta^2} \left[\frac{1}{2} \ln \frac{2 m_e c^2 \gamma^2 \beta^2}{I^2} T^{max} - \beta^2 - \frac{\delta}{2} \right]$$

- dE/dx in [MeV g^{-1} cm^2]
- dE/dx depends only on β, independent of m
- Formula takes into account energy transfers

$I \leq dE \leq T^{max}$ $\quad$ I : mean excitation potential

$I \approx I_0 Z$ with $I_0 = 10$ eV $\quad$ (rough approximation, I fitted for each element)

- Bethe-Bloch formula only valid for "heavy" particles ($m \geq m_\mu$).
- Electrons and positrons need special treatment ($m_{proj}=m_{target}$), in addition Bremsstrahlung!

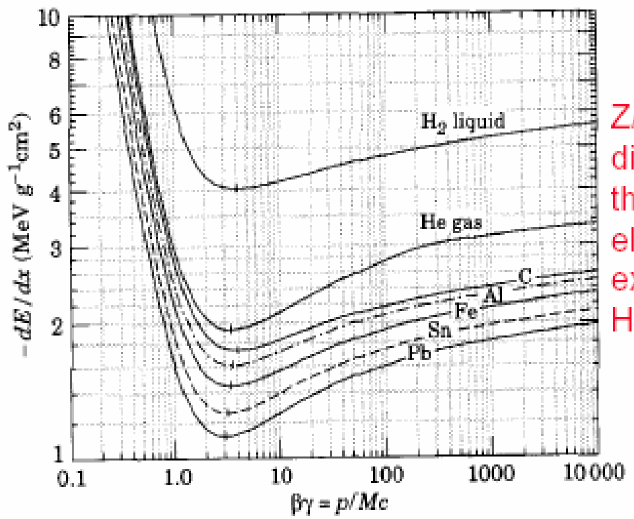

Z/A does not differ much for the various elements, except for Hydrogen!

$$\left\langle \frac{dE}{dx} \right\rangle = -4\pi N_A r_e^2 m_e c^2 z^2 \frac{Z}{A} \frac{1}{\beta^2} \left[\frac{1}{2} \ln \frac{2 m_e c^2 \gamma^2 \beta^2}{I^2} T^{\max} - \beta^2 - \frac{\delta}{2} \right]$$

- dE/dx first falls $\propto$ $1/\beta^2$ (more precise $\beta^{-5/3}$), kinematic factor
- then minimum at $\beta\gamma \approx 4$ (minimum ionizing particles, MIP)

  (dE/dx $\approx$ 1 - 2 MeV g^{-1} cm^2)
- then again rising due to $\ln \gamma^2$ term, relativistic rise, attributed to relativistic expansion of transverse E-field $\rightarrow$ contributions from more distant collisions.
- relativistic rise cancelled at high γ by "density effect", polarization of medium screens more distant atoms. Parameterized by δ (material dependent) $\rightarrow$ Fermi plateau
- many other small corrections

Measured and calculated dE/dx

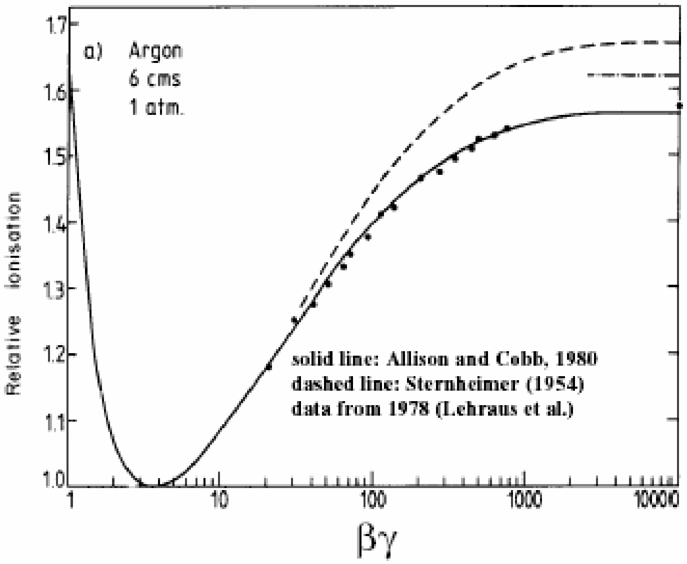

Primary and total ionization

Fast charged particles ionize the atoms of a gas.

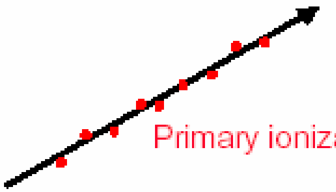

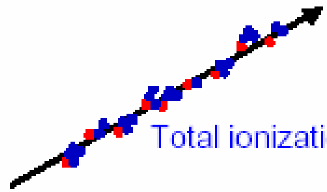

Often the resulting primary electron will have enough kinetic energy to ionize other atoms.

$$n_{total} = \frac{\Delta E}{W_i} = \frac{\frac{dE}{dx}\Delta x}{W_i}$$

$$n_{total} \approx 3\ldots4 \cdot n_{primary}$$

total number of created electron-ion pairs.
ΔE = total energy loss
W_i = effective <energy loss>/pair

Number of primary electron/ion pairs in frequently used (detector) gases.

(Lohse and Witzeling, Instrumentation In High Energy Physics, World Scientific, 1992)

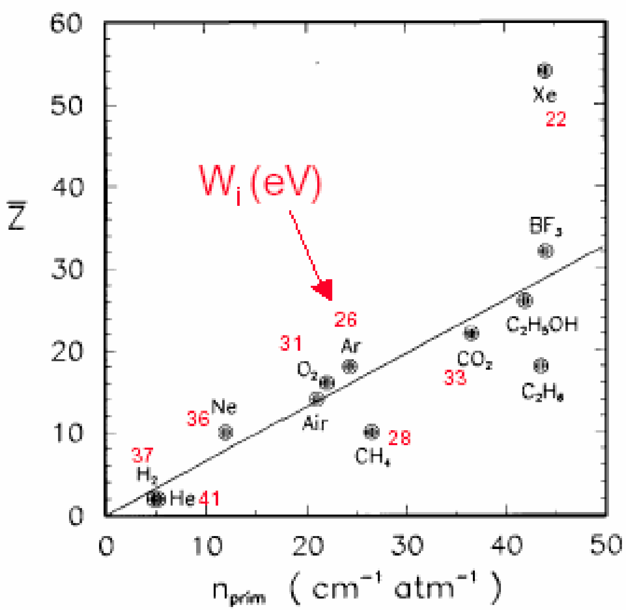

≈ 100 electron-ion pairs are not easy to detect!

Noise of amplifier ≈1000 e^- (ENC) !

We need to increase the number of e-ion pairs.

Gas amplification

Consider cylindrical field geometry (simplest case):

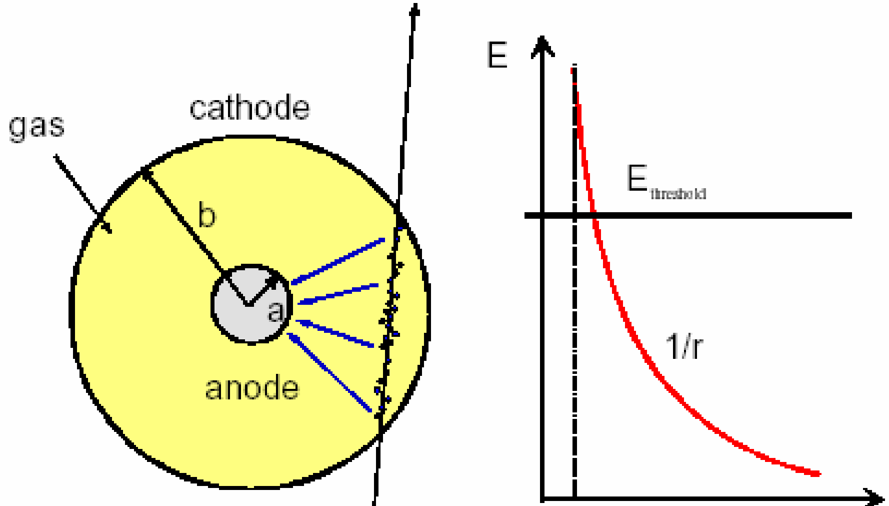

$$E(r) = \frac{CV_0}{2\pi\varepsilon_0} \cdot \frac{1}{r}$$

$$V(r) = \frac{CV_0}{2\pi\varepsilon_0} \cdot \ln\frac{r}{a}$$

C = capacitance / unit length

Electrons drift towards the anode wire (≈ stop and go! More details in next lecture!).

Close to the anode wire the field is sufficiently high (some kV/cm), so that e^- gain enough energy for further ionization → exponential increase of number of e^--ion pairs.

Choice of gas:

Dense noble gases. Energy dissipation mainly by ionization! High specific ionization.

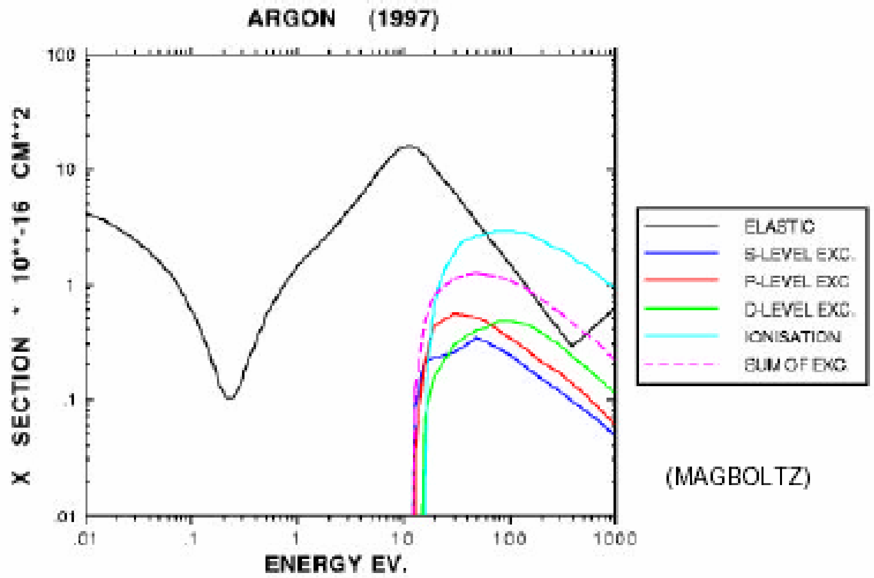

De-excitation of noble gases only possible via emission of photons, e.g. 11.6 eV for Argon.

This is above ionization threshold of metals, e.g. Copper 7.7 eV.

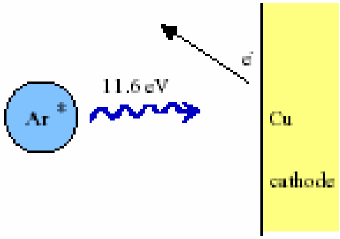

→ new avalanches → permanent discharges !

Solution: Add poly-atomic gases as quenchers.

Absorption of photons in a large energy range (many vibrational and rotational energy levels).

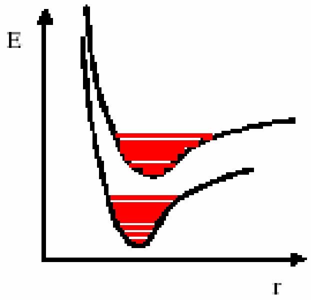

Energy dissipation by collisions or dissociation into smaller molecules.

Methane: absorption band 7.9 - 14.5 eV

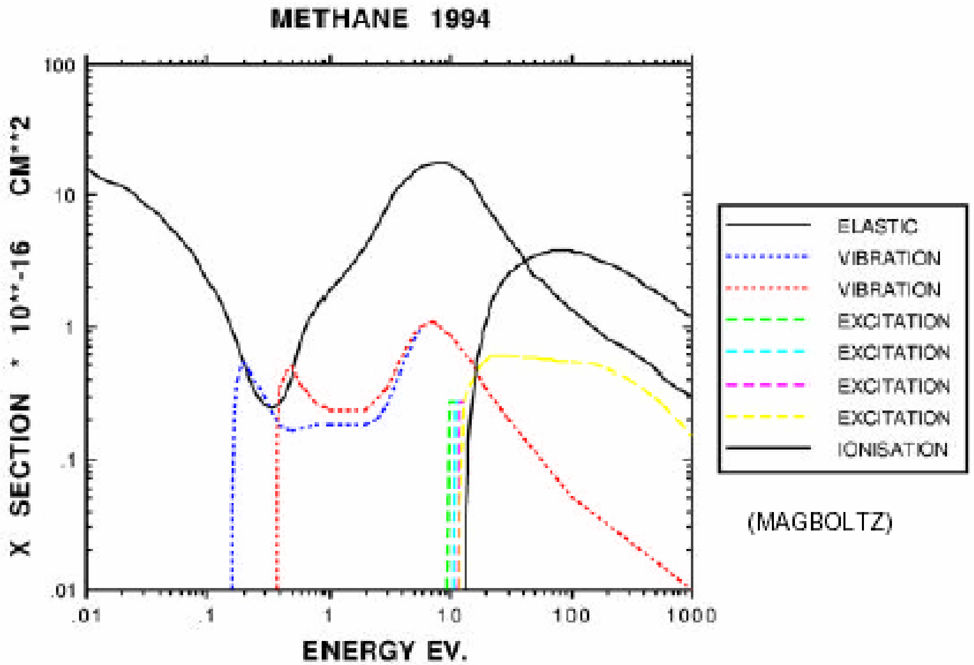

Signal formation

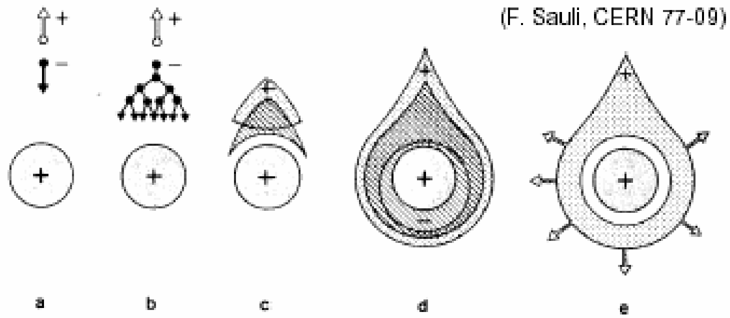

Avalanche formation within a few wire radii and within t < 1 ns!

Signal induction both on anode and cathode due to moving charges (both electrons and ions).

$$dv = \frac{Q}{lCV_0}\frac{dV}{dr}dr$$

Electrons collected by anode wire, i.e. *dr* is small (few μm). Electrons contribute only very little to detected signal (few %).

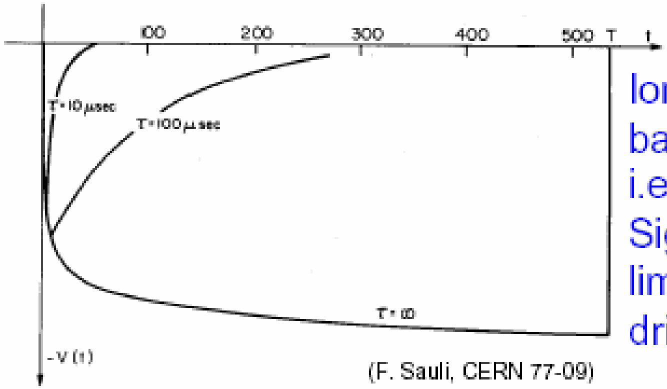

Ions have to drift back to cathode, i.e. *dr* is big. Signal duration limited by total ion drift time !

Need electronic signal differentiation to limit dead time.

Operation modes:

- ionization mode: full charge collection, but no charge multiplication.
- Proportional mode: above threshold voltage multiplication starts. Detected signal proportional to original ionization → energy measurement (dE/dx). Secondary avalanches have to be quenched. Gain 10^4 - 10^5.
- Limited Proportional → Saturated → Streamer mode: Strong photo-emission. Secondary avalanches, merging with original avalanche. Requires strong quenchers or pulsed HV. High gain (10^{10}), large signals → simple electronics.
- Geiger mode: Massive photo emission. Full length of anode wire affected. Stop discharge by cutting down HV. Strong quenchers needed as well.

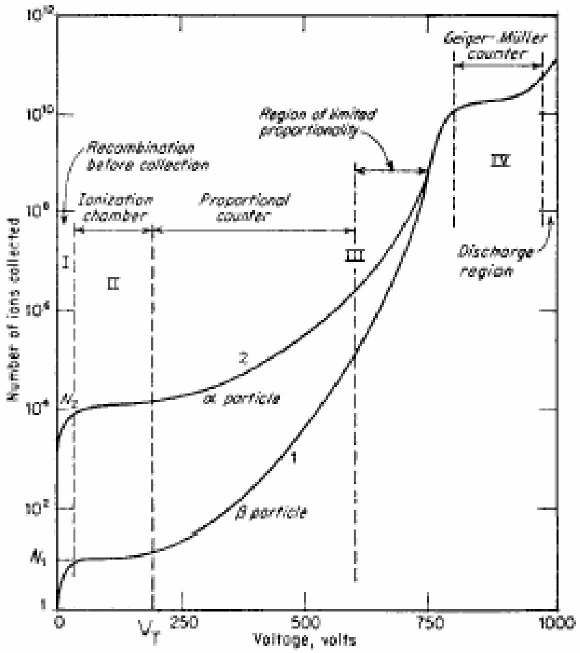

Drift chambers

(First studies: T. Bressani, G. Charpak, D. Rahm, C. Zupancic, 1969
First operation drift chamber: A.H. Walenta, J. Heintze, B. Schürlein, NIM 92 (1971) 373)

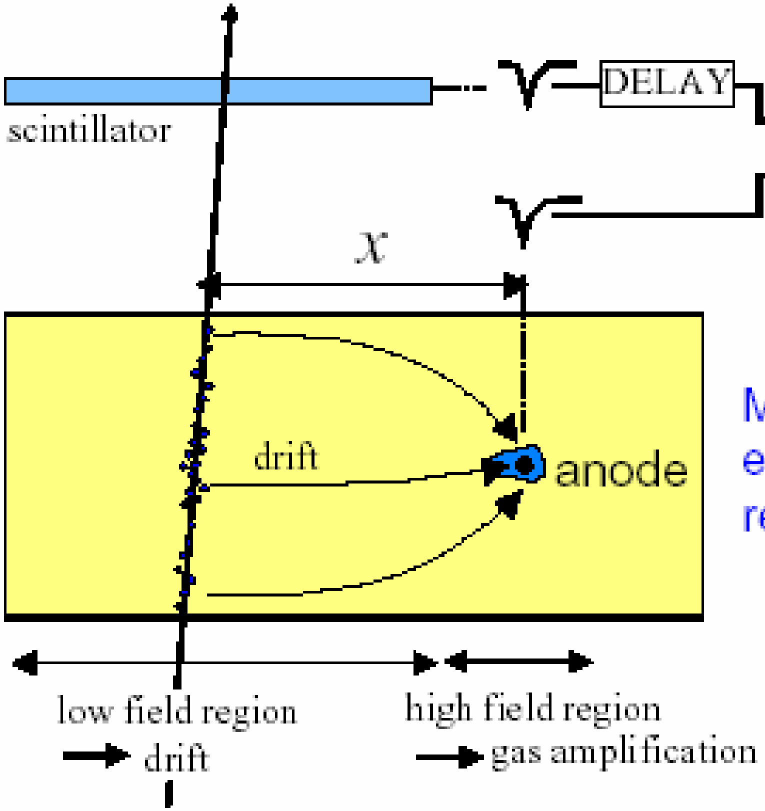

Measure arrival time of electrons at sense wire relative to a time t_0.

$$x = \int v_D(t)\,dt$$

Cherenkov radiation

Cherenkov radiation is emitted when a charged particle passes a dielectric medium with velocity

$$\beta \geq \beta_{thr} = \frac{1}{n} \quad n: \text{refractive index}$$

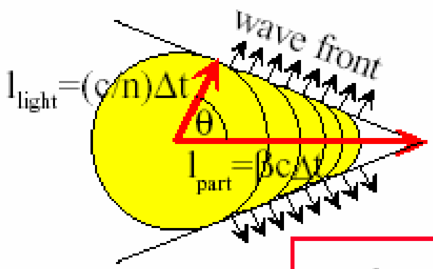

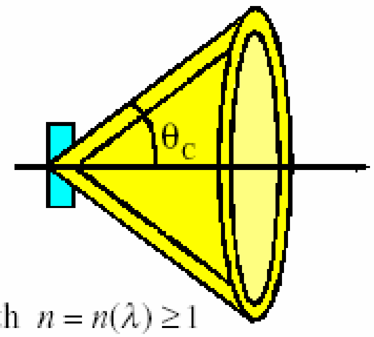

$$\cos\theta_C = \frac{1}{n\beta} \quad \text{with} \quad n = n(\lambda) \geq 1$$

$$\beta_{thr} = \frac{1}{n} \rightarrow \theta_C \approx 0$$ threshold

$$\theta_{max} = \arccos\frac{1}{n}$$ 'saturated' angle (β=1)

Number of emitted photons per unit length and unit wavelength interval

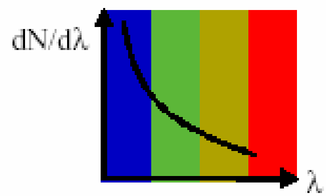

$$\frac{d^2N}{dxd\lambda} = \frac{2\pi z^2\alpha}{\lambda^2}\left(1-\frac{1}{\beta^2 n^2}\right) = \frac{2\pi z^2\alpha}{\lambda^2}\sin^2\theta_C$$

$$\frac{d^2N}{dxd\lambda} \propto \frac{1}{\lambda^2} \quad \text{with} \quad \lambda = \frac{c}{\nu} = \frac{hc}{E} \qquad \frac{d^2N}{dxdE} = const.$$

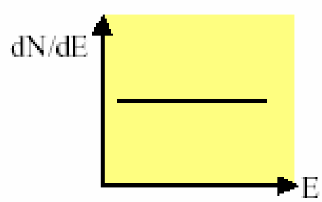

Transition radiation detectors

(there is an excellent review article by B. Dolgoshein (NIM A 326 (1993) 434))

TR predicted by Ginzburg and Franck in 1946

Electromagnetic radiation is emitted when a charged particle traverses a medium with a discontinuous refractive index, e.g. the boundaries between vacuum and a dielectric layer.

A (too) simple picture

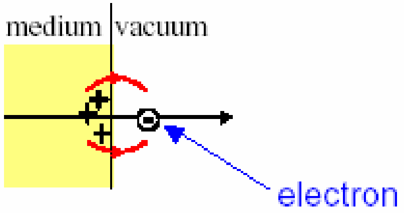

A correct relativistic treatment shows that…

(G. Garibian, Sov. Phys. JETP63 (1958) 1079)

- Radiated energy per medium/vacuum boundary

$$W = \frac{1}{3}\alpha\hbar\omega_p\gamma \qquad \boxed{W \propto \gamma}$$

→ Only high energy $e^{\pm}$ will emit TR. Identification of $e^{\pm}$

$$\omega_p = \sqrt{\frac{N_e e^2}{\varepsilon_0 m_e}} \qquad \begin{pmatrix}\text{plasma}\\ \text{frequency}\end{pmatrix} \qquad \hbar\omega_p \approx 20\text{eV (plastic radiators)}$$

- Number of emitted photons / boundary is small

$$N_{ph} \approx \frac{W}{\hbar\omega} \propto \alpha \approx \frac{1}{137}$$

Need many transitions → build a stack of many thin foils with gas gaps

- X-rays are emitted with a sharp maximum at small angle

$$\theta \propto 1/\gamma$$

→ TR stay close to track

- Emission spectrum of TR

Typical energy: $\hbar\omega \approx \frac{1}{4}\hbar\omega_p\gamma$

→ photons in the keV range

- Simulated emission spectrum of a CH_2 foil stack

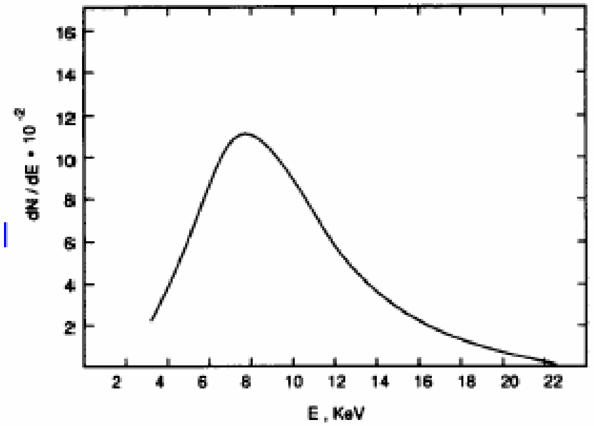

TRT Barrel & End-cap

Detecting element: straw tube 4 mm diam., 30 μm W/Au wire

Robust operation conditions: safe and fast gas

$Xe(70\%)+CO_2(20\%)+CF_4(10\%)$:TDR

$Xe(70\%)+CO_2(20\%)+O_2(10\%)$

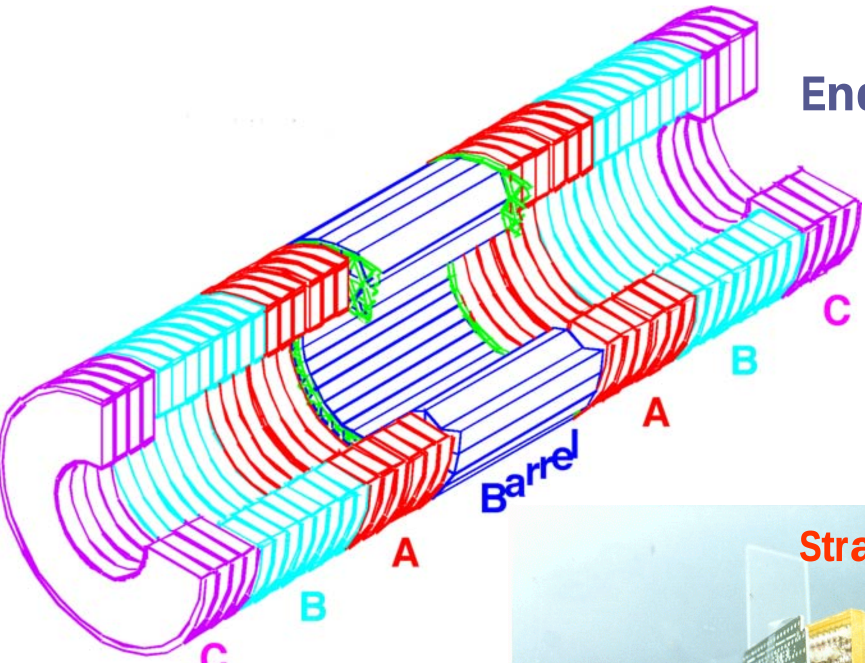

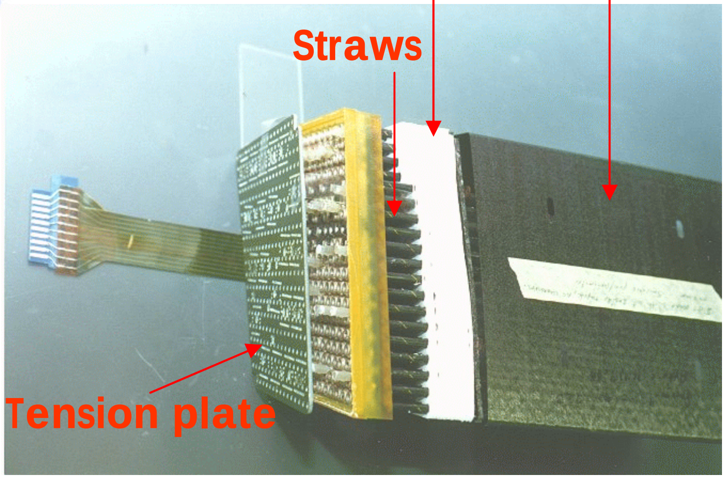

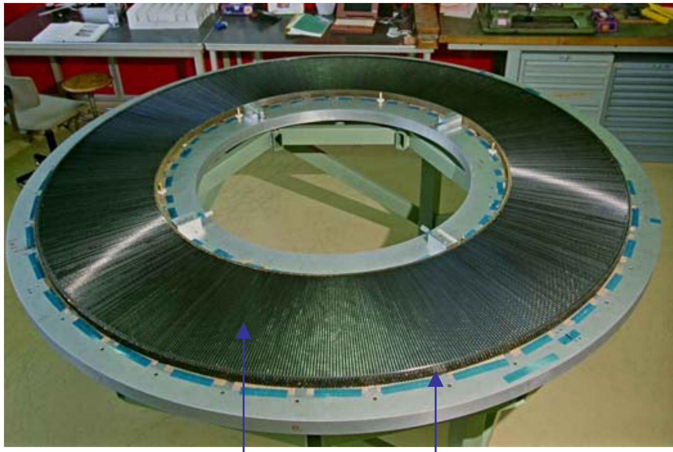

TRT Barrel & End-cap

Detecting element

Straw Tube 4 mm O.D.

30 μm W/Au wire

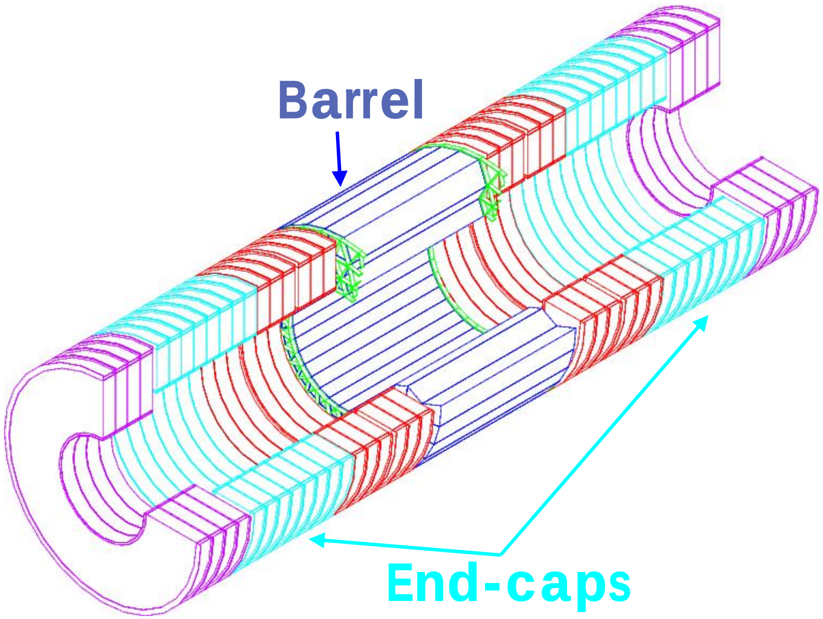

	BARREL	END-CAPs
Geometry	Linear	Radial
Straw length	144 cm	39 cm (End-cap A&B) 52 cm (End-cap C)
Nb electronic channels	~ 100 000	~ 320 000

TRT

TRT Barrel Module Types

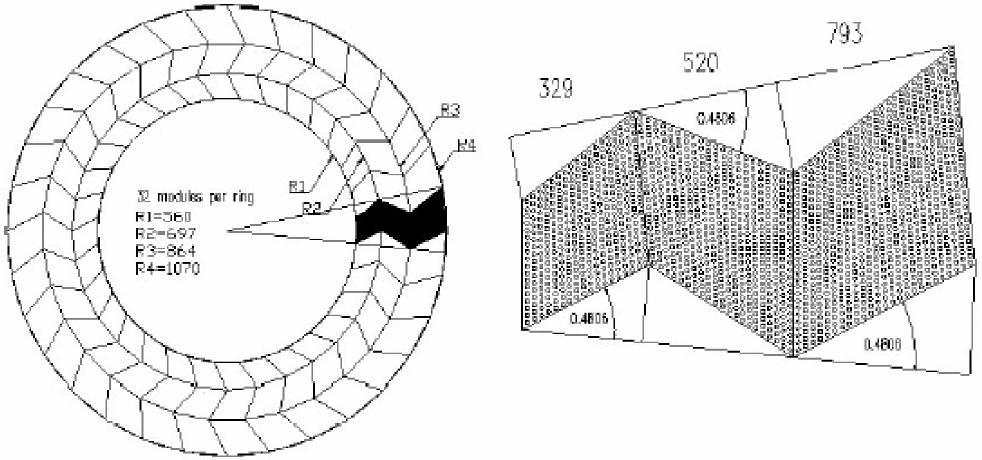

	Type 1	Type 2	Type 3
Number of Modules	32	32	32
Straws per Module	329	520	793
Straw Layer Number	19	24	30
Inner Radius (mm)	560	697	864
Outer Radius (mm)	697	864	1070

- Entire barrel is divided into 3 rings of 32 modules.
- Straws are distributed for a continuous tracking geometry
- 52,544 straws,
  105,088 readout channels
- Average number of straws crossed by a track = 36, out of 73 layers
- Average number of TR-hits for 20GeV Pt electron = 7

TRT

TRT Barrel Module

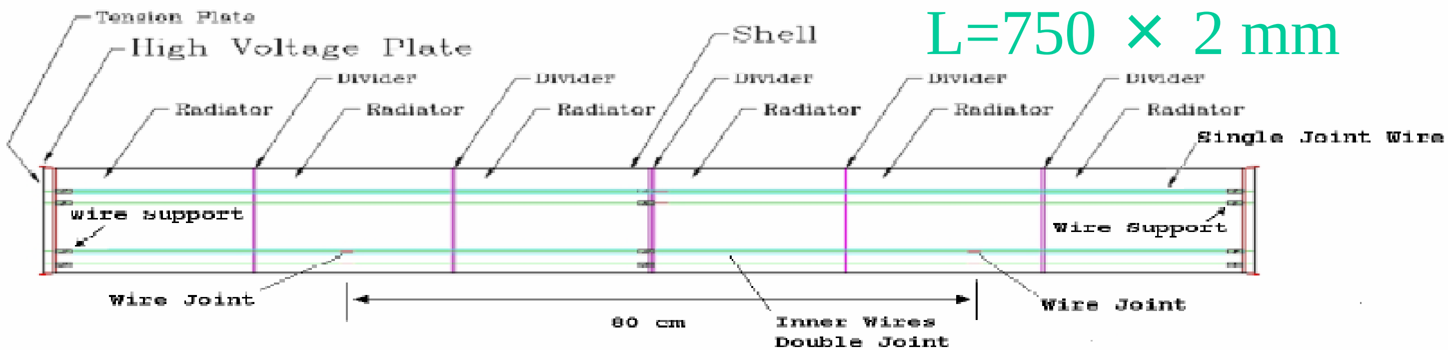

- **Sense wires are split in half to reduce counting rate.**
- **This is not enough for the 11 inner most layers of wires!**
- **±40cm from the center of these wires are deadened by using 2 wire joints.**
- **All straws are the same, but there are 2 different kinds of wires: "Single joint" & "Double Joint"**

Barrel straw

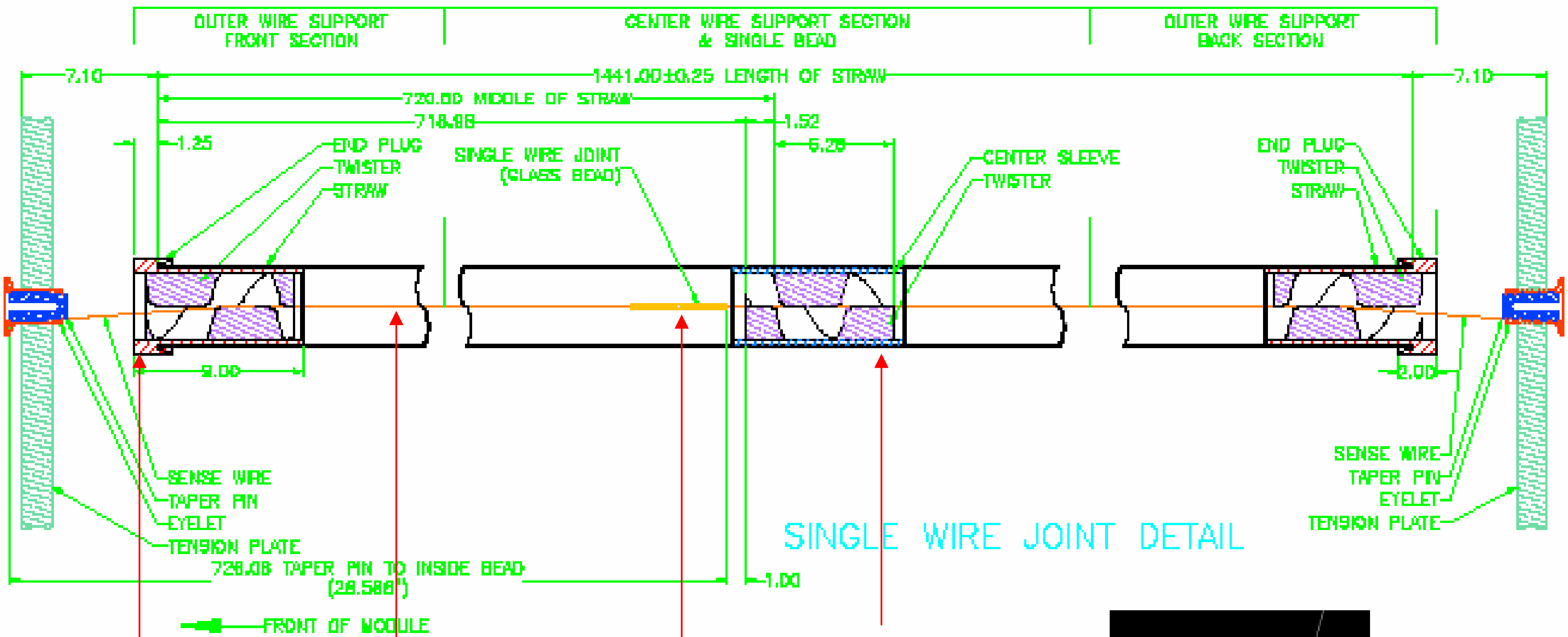

Twister

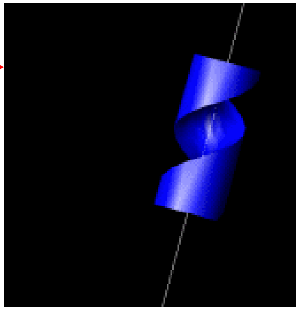

End plug

Wire
30 μm

Wire joint

Both end-cap and barrel use the same straws

(initially 166 cm long)

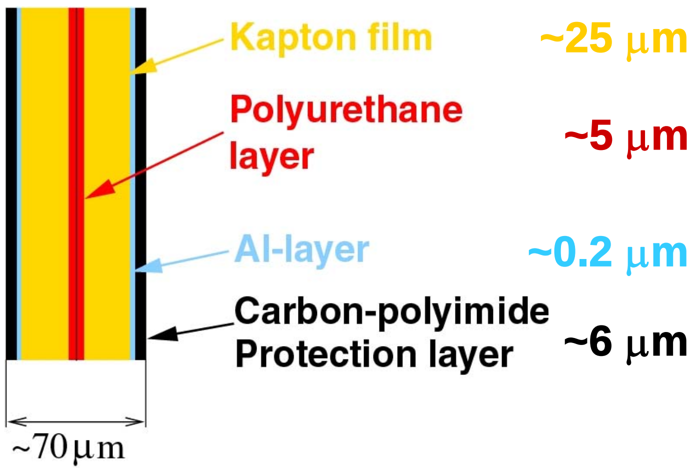

Straw wall (after winding)

R < 10 Ω/square

Straws are reinforced at PNPI and JINR (Russia)

In order to make straw rigid 4 C-fibres are attached along the straw

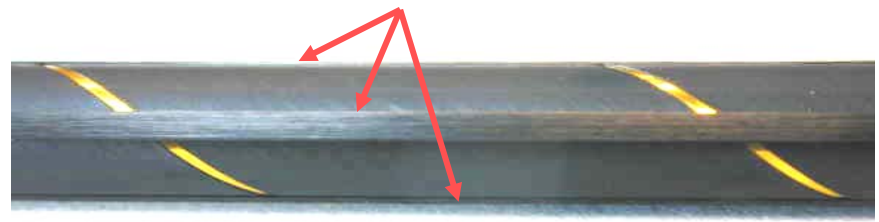

Reinforcement QC

Test	Yield (%)
Straw straightness	99.9
Outer diameter	99.9
Total Losses*	~ 1%

Barrel TRT Radiator

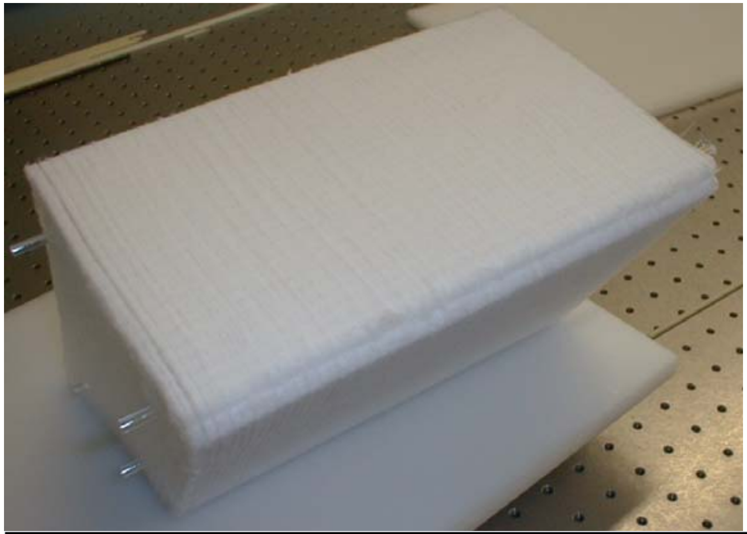

Stacks of polypropylene fiber sheets
Fiber is 15 mm diameter
Packed to 66 mg/cm^3 density

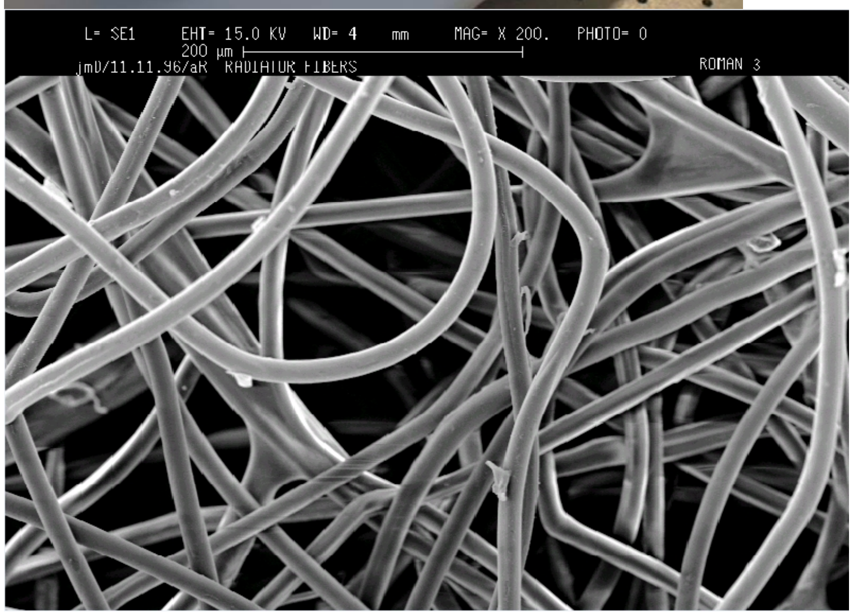

200um

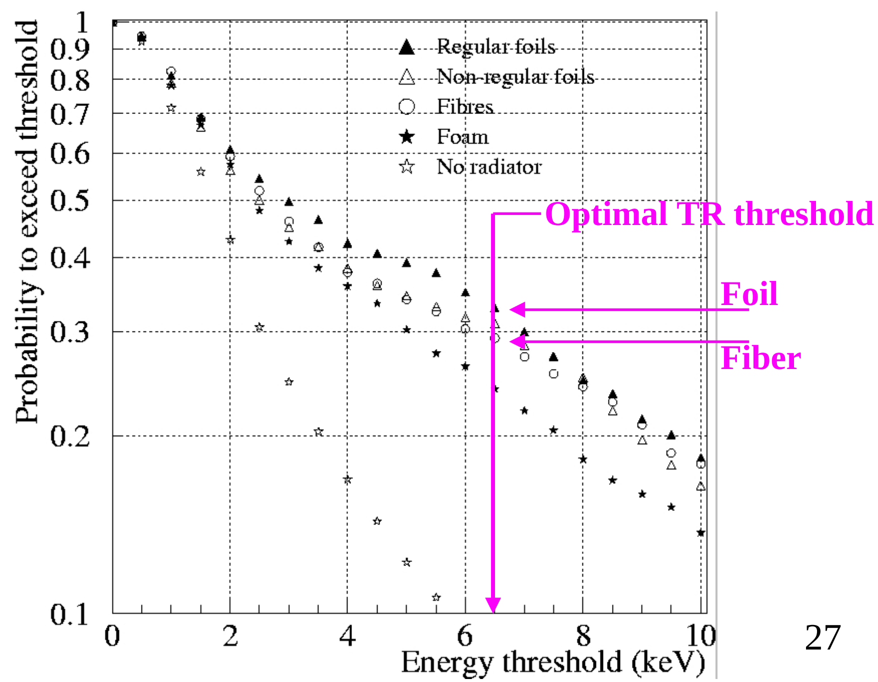

❑TRT End Cap Radiators are

- Stack of Polypropylene foils of 15 µm thickness

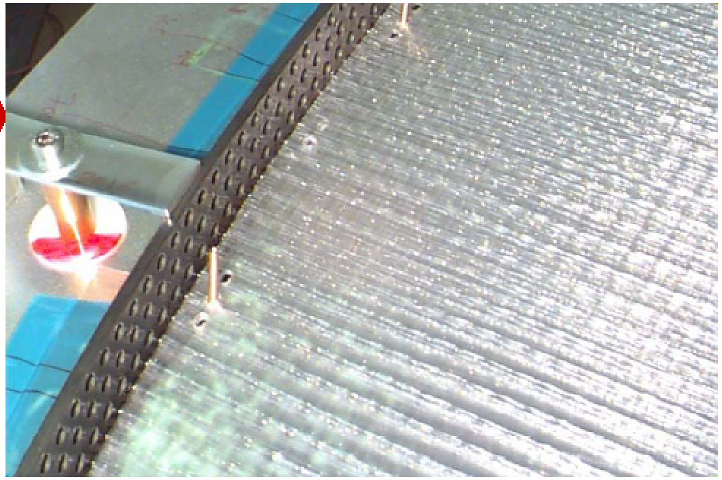

- Spacers (200 µm) between foils made from Polypropylene mesh

End-cap TRT Spacer

Cell size ~ 10mm x 10mm

10% of radiator material
"Haute couture" technology

Filament diam. ~ 15-20 mm

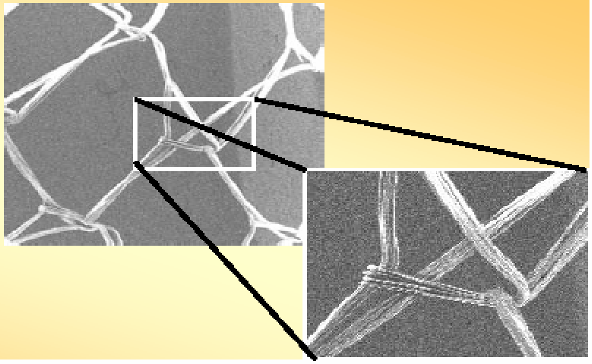

❑Procurement of TRT Radiators type A&B from *JENIFER* completed on 2002

TRT

TRT Read-out: Architecture

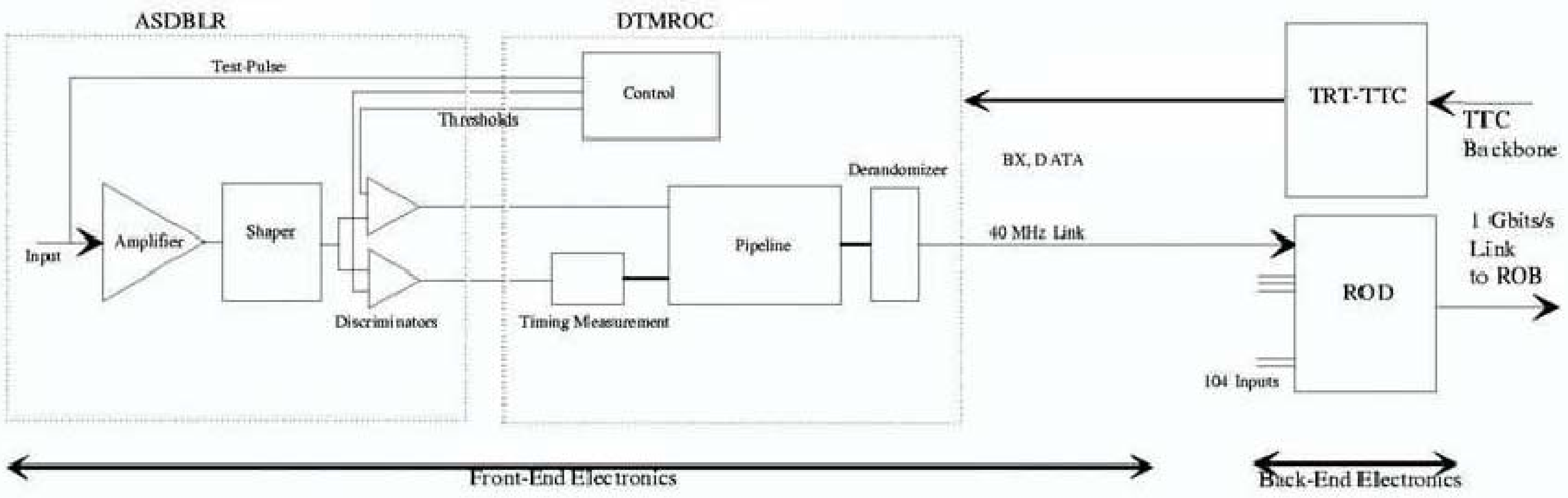

- Nominal gas gain: $2.5\ 10^4$
  - Drift time (DT): 250 eV (2 fC) threshold
  - Transition radiation (TR): 5 keV threshold

3n digitize
$\rightarrow$ 170 μ m

TRT

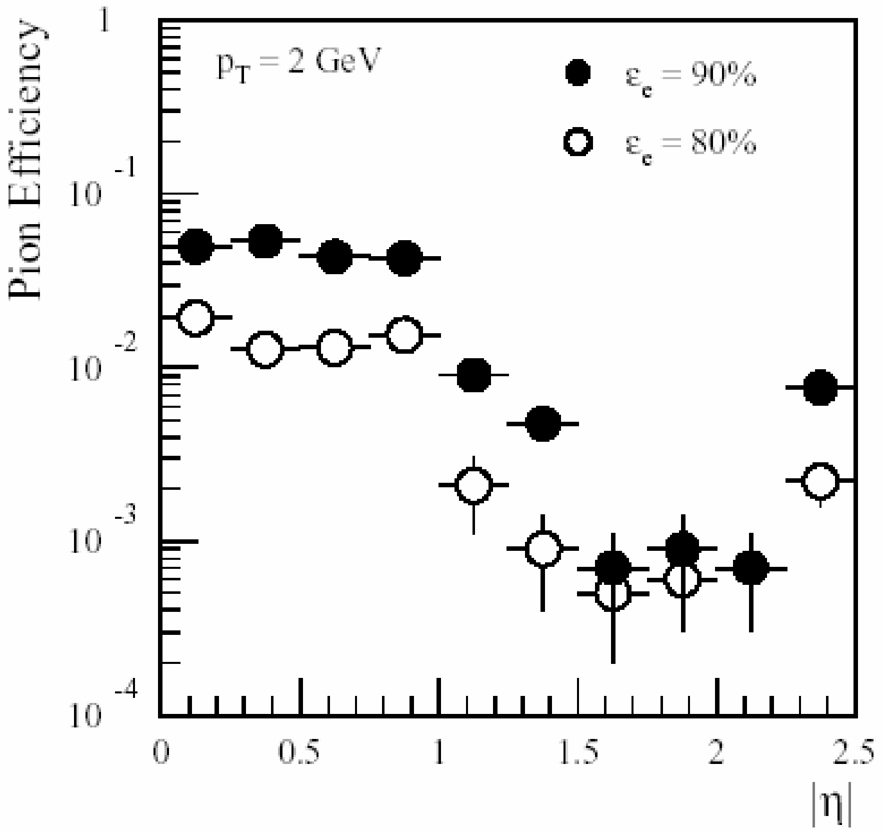

Figure 3-23 Pion efficiency as a function of |η| for p_T = 2 GeV for two different electron efficiencies. The efficiencies are relative; to get the total efficiency, the values must be multiplied by the efficiencies to pass the extended track quality cuts.

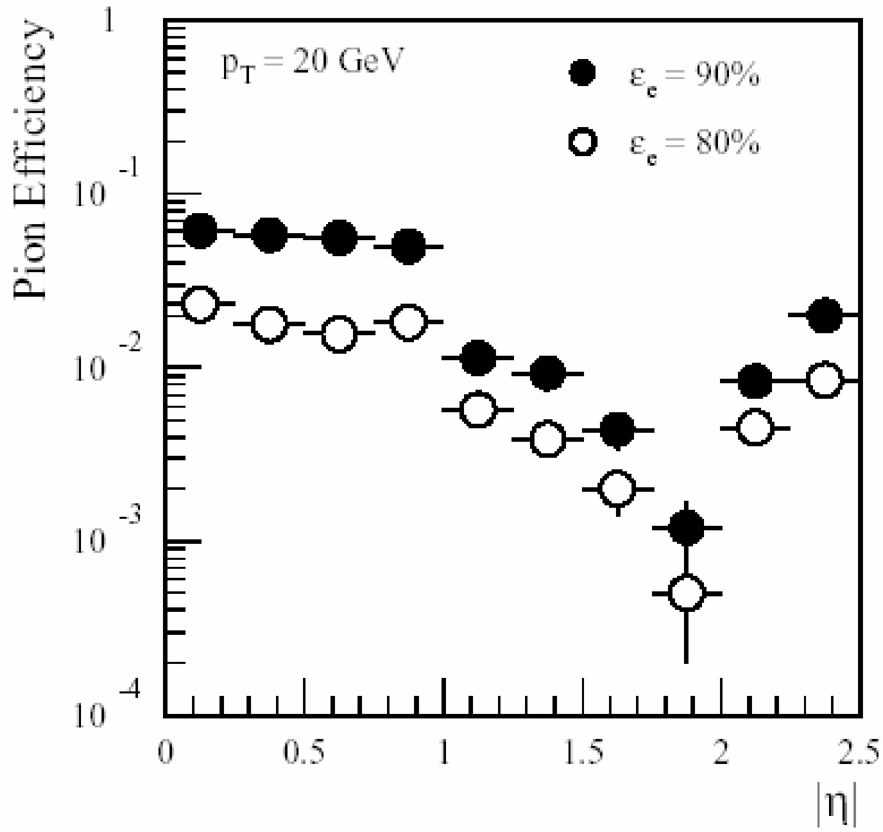

Figure 3-24 Pion efficiency as a function of |η| for p_T = 20 GeV for two different electron efficiencies.

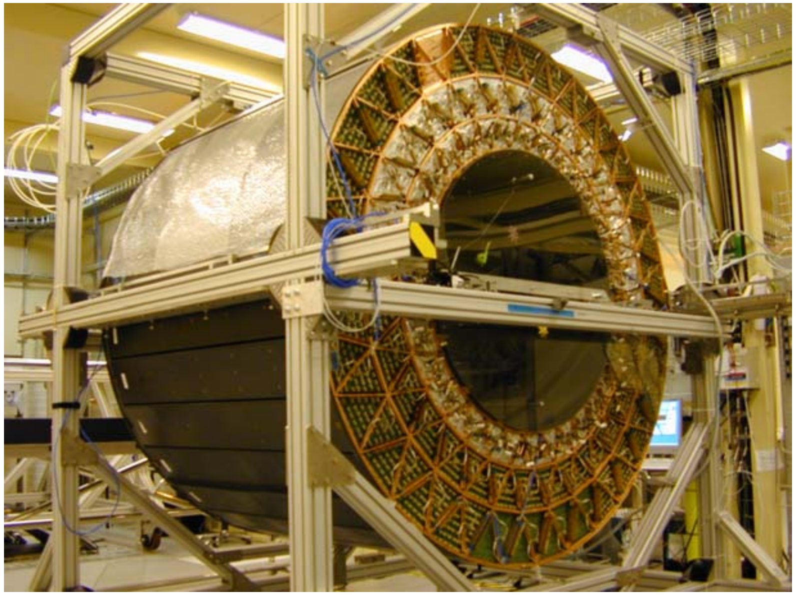

Barrel TRT

CERN SR1で組み立て中で殆ど完成。

Endcap TRT, A & C

- C側のwheelは全てCERNに到着。
- wheel stacking作業が始まった。
- 1.6%/年の率でHV-fuseが飛んでいる。

- TRT C-wheelsは2012年時に入れる

Silicon detectors

Solid state detectors have a long tradition for energy measurements (Si, Ge, Ge(Li)).

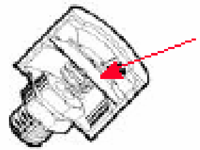

Si sensor

Here we are interested in their use as precision trackers !

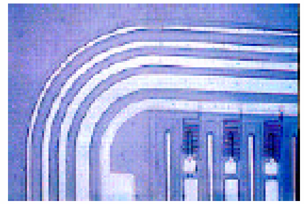

ATLAS SCT

Some characteristic numbers for silicon

- Band gap: E_g =1.12 V.
- E(e^--hole pair) = 3.6 eV, (≈ 30 eV for gas detectors).
- High specific density (2.33 g/cm^3) → ΔE/track length for M.I.P.'s.: 390 eV/μm ≈ 108 e-h/ μm (average)
- High mobility: μ_e =1450 cm^2/Vs, μ_h = 450 cm^2/Vs
- Detector production by microelectronic techniques → small dimensions → fast charge collection (<10 ns).
- Rigidity of silicon allows thin self supporting structures. Typical thickness 300 μm → ≈ 3.2 ·10^4 e-h (average)
- But: No charge multiplication mechanism!

How to obtain a signal ?

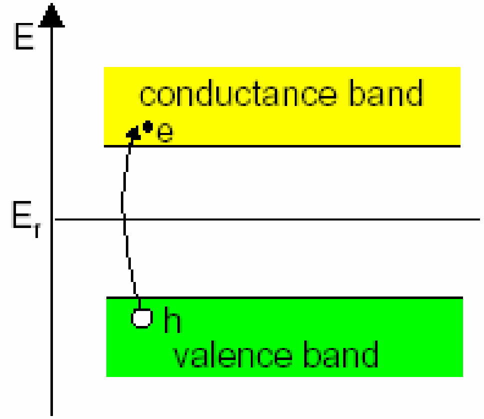

In a pure intrinsic (undoped) material the electron density n and hole density p are equal. $n = p = n_i$

For Silicon: $n_i \approx 1.45 \cdot 10^{10}\ cm^{-3}$

In this volume we have $4.5 \cdot 10^8$ free charge carriers, but only $3.2 \cdot 10^4$ e-h pairs produced by a M.I.P.

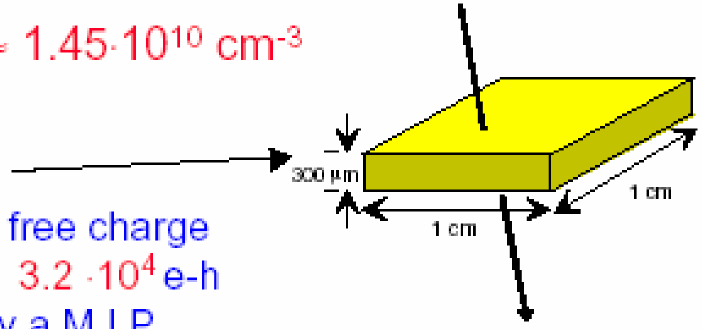

→ Reduce number of free charge carriers, i.e. deplete the detector

Most detectors make use of reverse biased p-n junctions

Doping

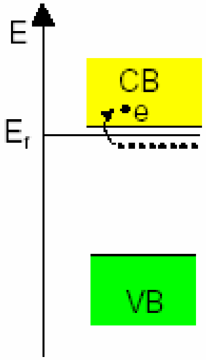

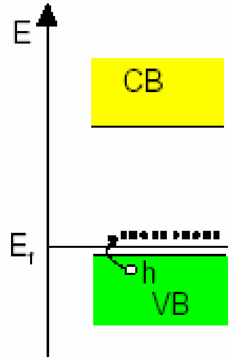

n-type: Add elements from V^{th} group, donors, e.g. As. Electrons are the majority carriers.

p-type: Add elements from III^{rd} group, acceptors, e.g. B. Holes are the majority carriers.

	detector grade	electronics grade
doping concentration	10^{12} cm^{-3} (n) - 10^{15} cm^{-3} (p^+)	$10^{17(18)}$ cm^{-3}
resistivity	≈ 5 kΩ·cm	≈1 Ω·cm

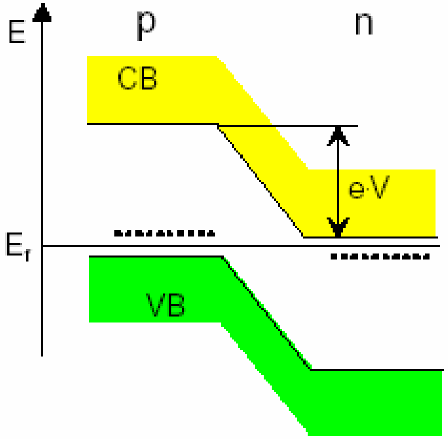

pn junction

There must be a single Fermi level ! Deformation of band structure → potential difference.

I型半導体
(真性半導体)

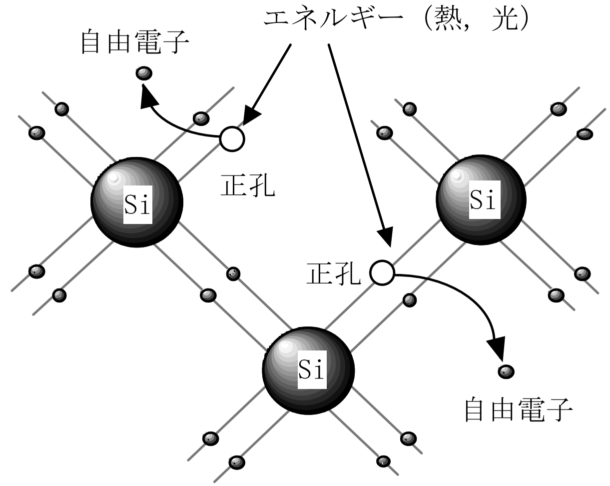

図2-4　電子ー正孔対の生成

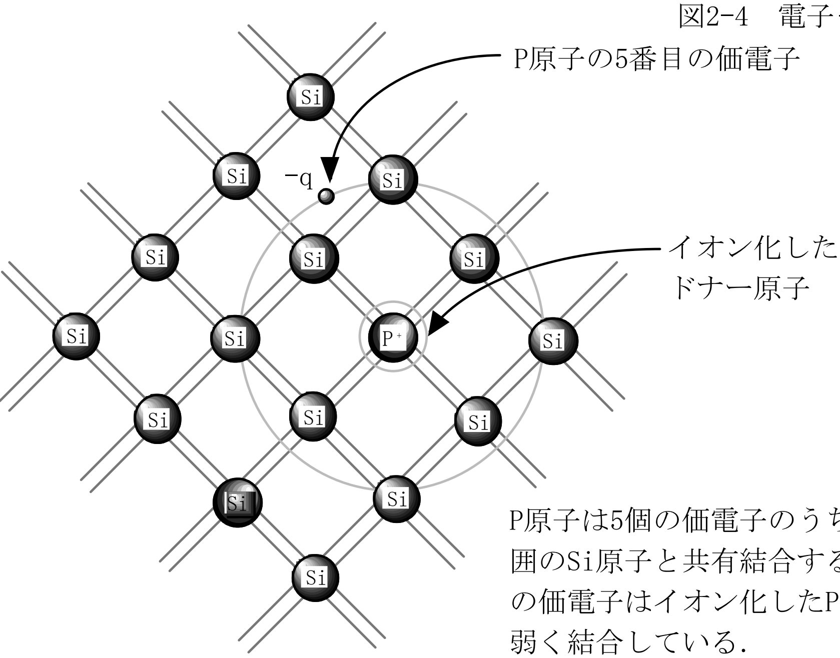

P原子は5個の価電子のうち4個で周囲のSi原子と共有結合する．第5番目の価電子はイオン化したP^+イオンに弱く結合している．

図2-5　n形半導体

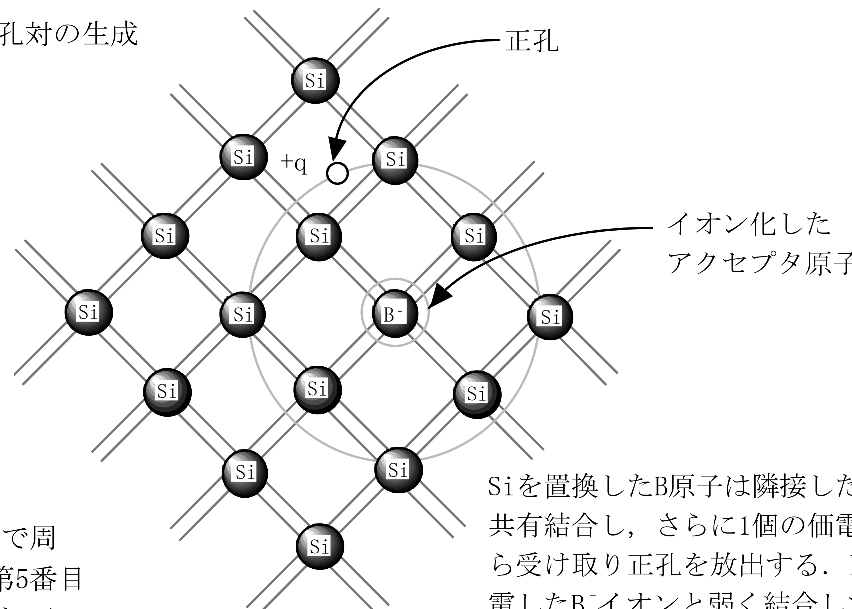

Siを置換したB原子は隣接した3個のSiと共有結合し，さらに1個の価電子を周囲から受け取り正孔を放出する．正孔は負に帯電したB^-イオンと弱く結合している．

図2-6　p形半導体

THE PN JUNCTION

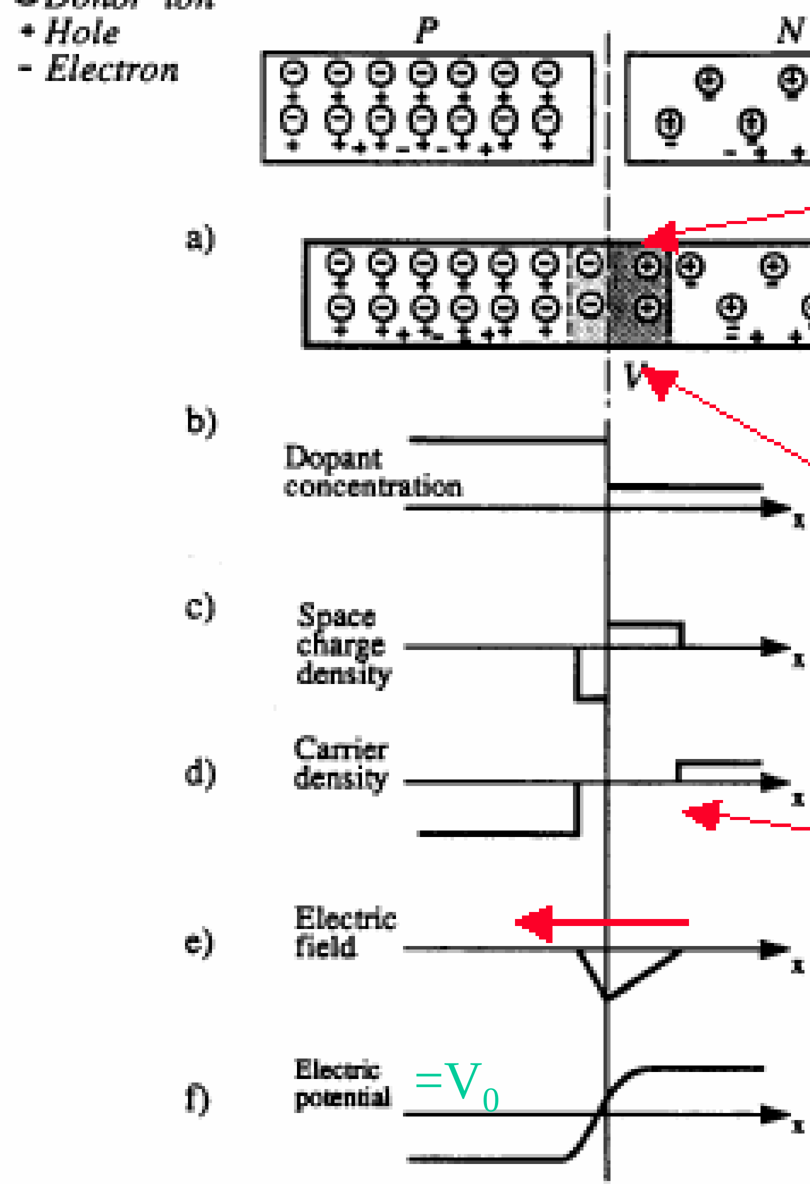

diffusion of e⁻ into p-zone, h⁺ into n-zone
→ potential difference stopping diffusion

$N_A > N_D$

thin depletion zone

$N_A x_p = N_D x_n$:x depth of depletion

N_D側に伸びる

no free charge carriers in depletion zone

(A. Peisert, Instrumentation In High Energy Physics, World Scientific)

$d = x_p + x_n \sim x_n = \sqrt{(2 \varepsilon V_0 / e N_D)}$

比抵抗ρを導入

$1/\rho \sim e\mu N_D$　　　　　(μ :移動度)

$d = x_p + x_n \sim x_n = \sqrt{(2\varepsilon V_0 / e N_D)}$

$= \sqrt{(2\varepsilon \rho \mu V_0)}$

$V_0 \sim 0.7V$:通常のダイオード

逆バイアスVをかけると　　　$V_0 \rightarrow V_0 + V$

Depletion layerは厚くなる　　　→信号大

d=300 μmをV〜100Vで得るには

$\rho > 1K\Omega cm$

	detector grade	electronics grade
doping concentration	10^{12} cm^{-3} (n) - 10^{15} cm^{-3} (p^+)	$10^{17(18)}$ cm^{-3}
resistivity	≈ 5 kΩ·cm	≈1 Ω·cm

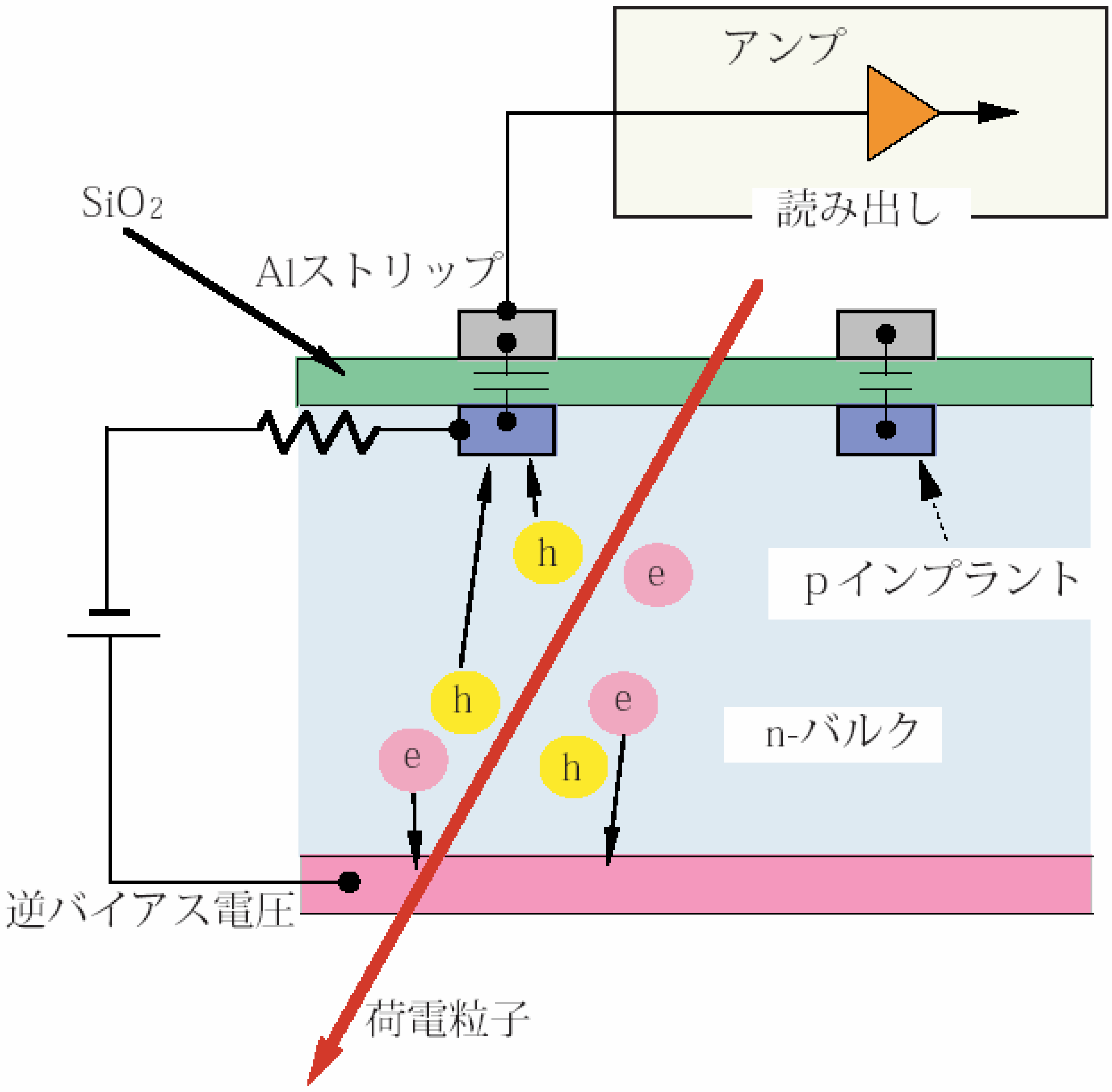
アンプ
読み出し
SiO2
Alストリップ
h
e
pインプラント
h
e
n-バルク
e
h
逆バイアス電圧
荷電粒子

Barrel Silicon microstrip detector (SCT ： Semiconductor Tracker)

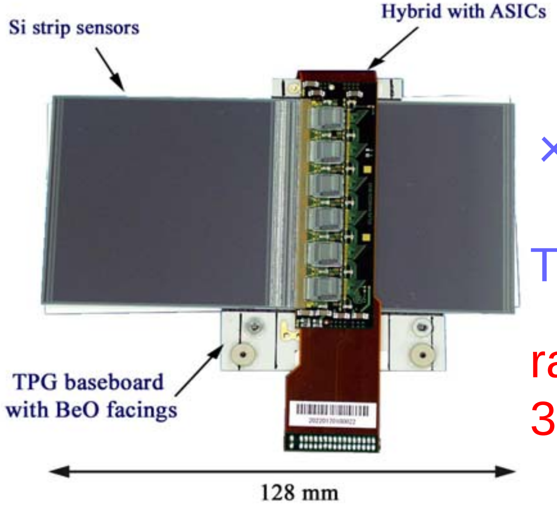

×2,112 modules →

Total area = $34m^2$

radiation tolerance
3×10^{14} n/cm^2 (10 years)

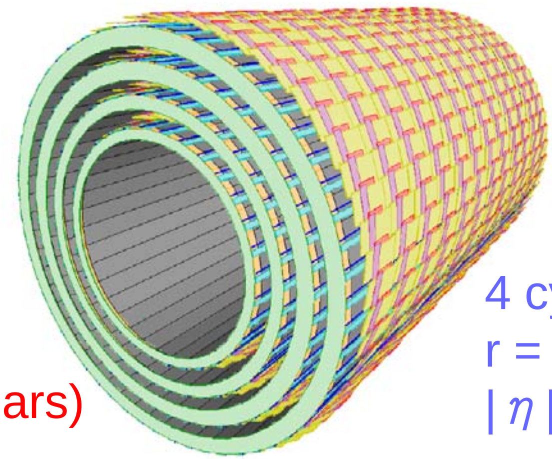

4 cylinders
r = 30~52cm
$|\eta|<1.4$

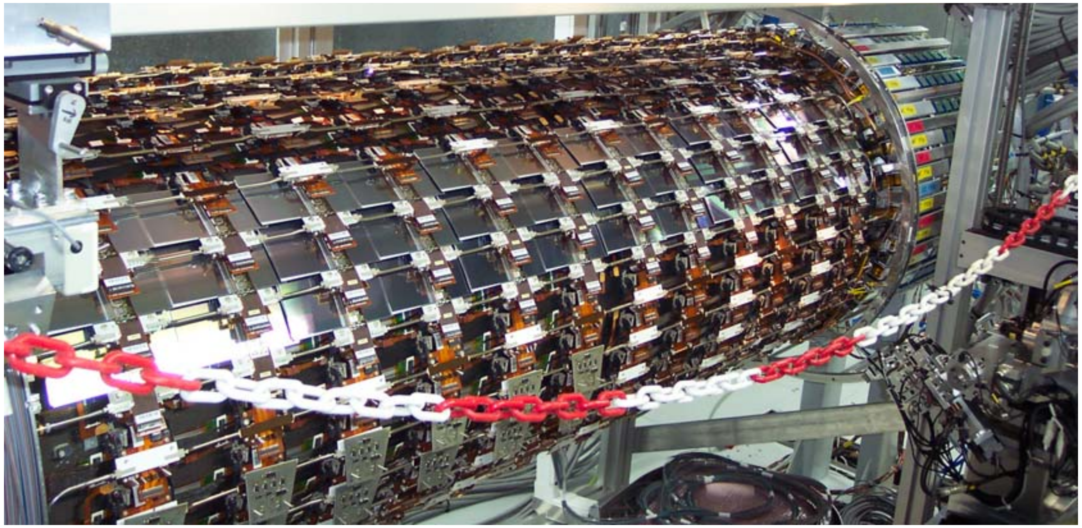

First complete barrel cylinder at Oxford U. December 2004
↓
CERN

Barrel SCT modules

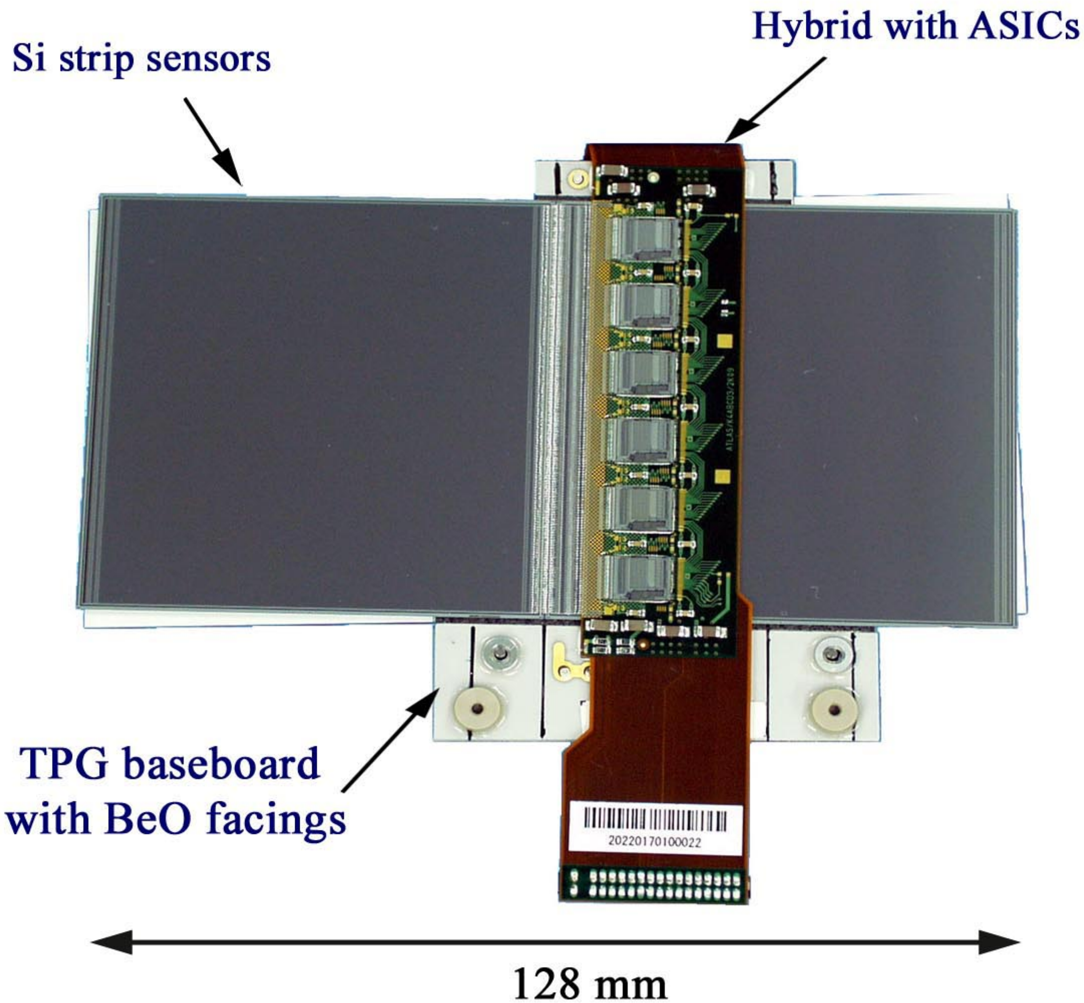

Specifications:

Strip pitch : 80 μm
Stereo angle : 40 mr $\rightarrow \Delta Z$:2 mm
readout channels ; 1536 ch
~ 5000 wire bondings
Assembly accuracy < 5 μm

Parts:

4 Silicon sensors (Hamamatsu)
12 ABCD chips (BiCMOS ASIC)
TPG thermal conductor (US)
Flexible hybrid circuit (Japan)

Fablication:

Total: 2600 modules
980 in Japan (best yield > 95%)
Others in UK, US and Scandinavia

Barrel SCT module 展開図

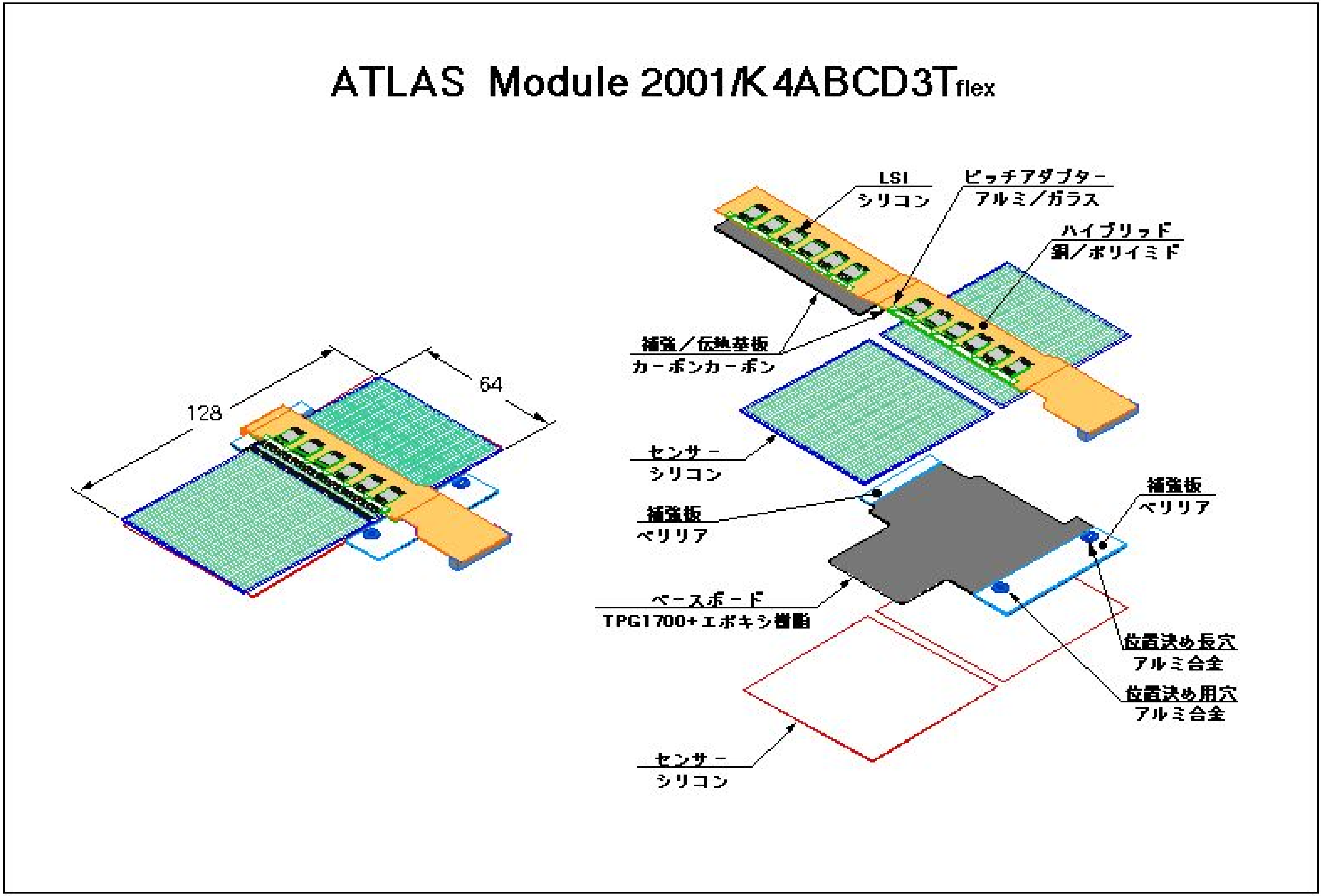

Forward SCT module

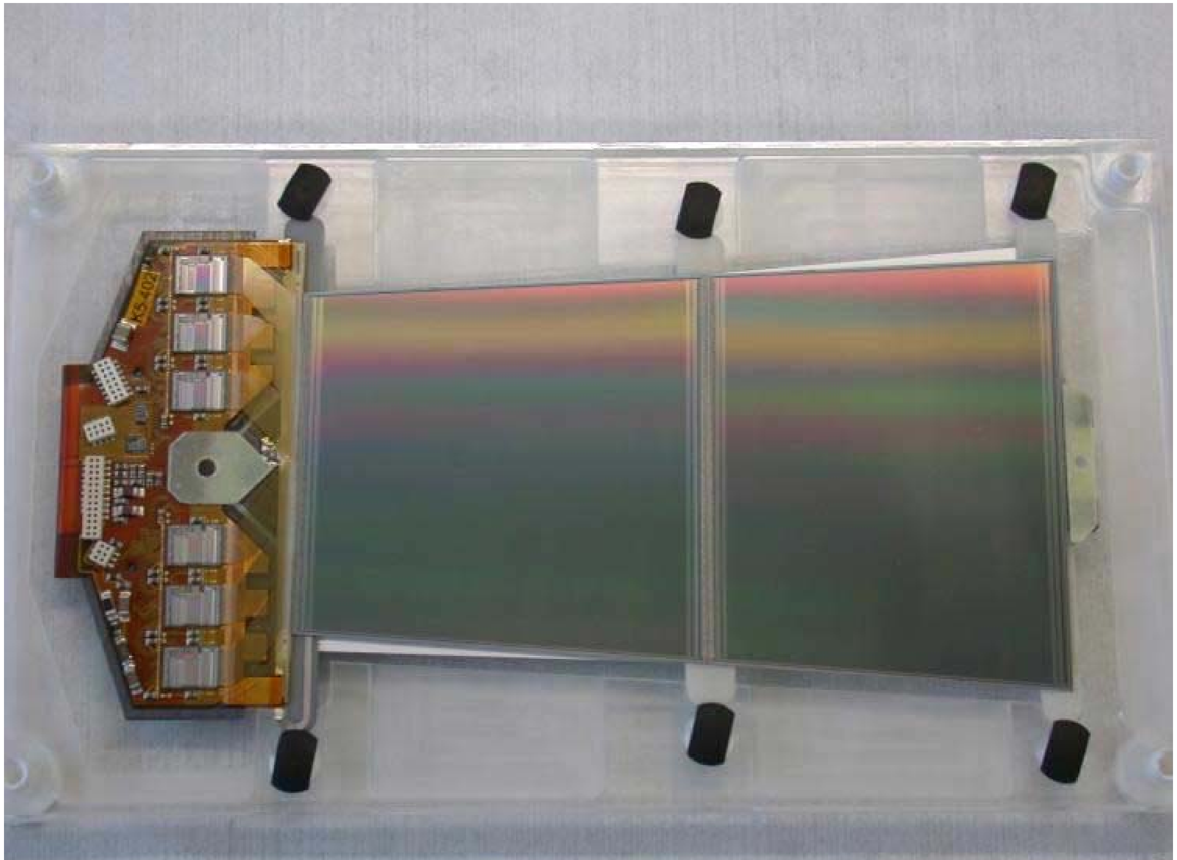

988 × 2 modules

Module size, two layers, 40mr stereo	768 strips, 12cm long
Strip pitch	54-69, 70-95, 71-90 μm
Radial range	260 mm - 560 mm

Barrel SCT sensor

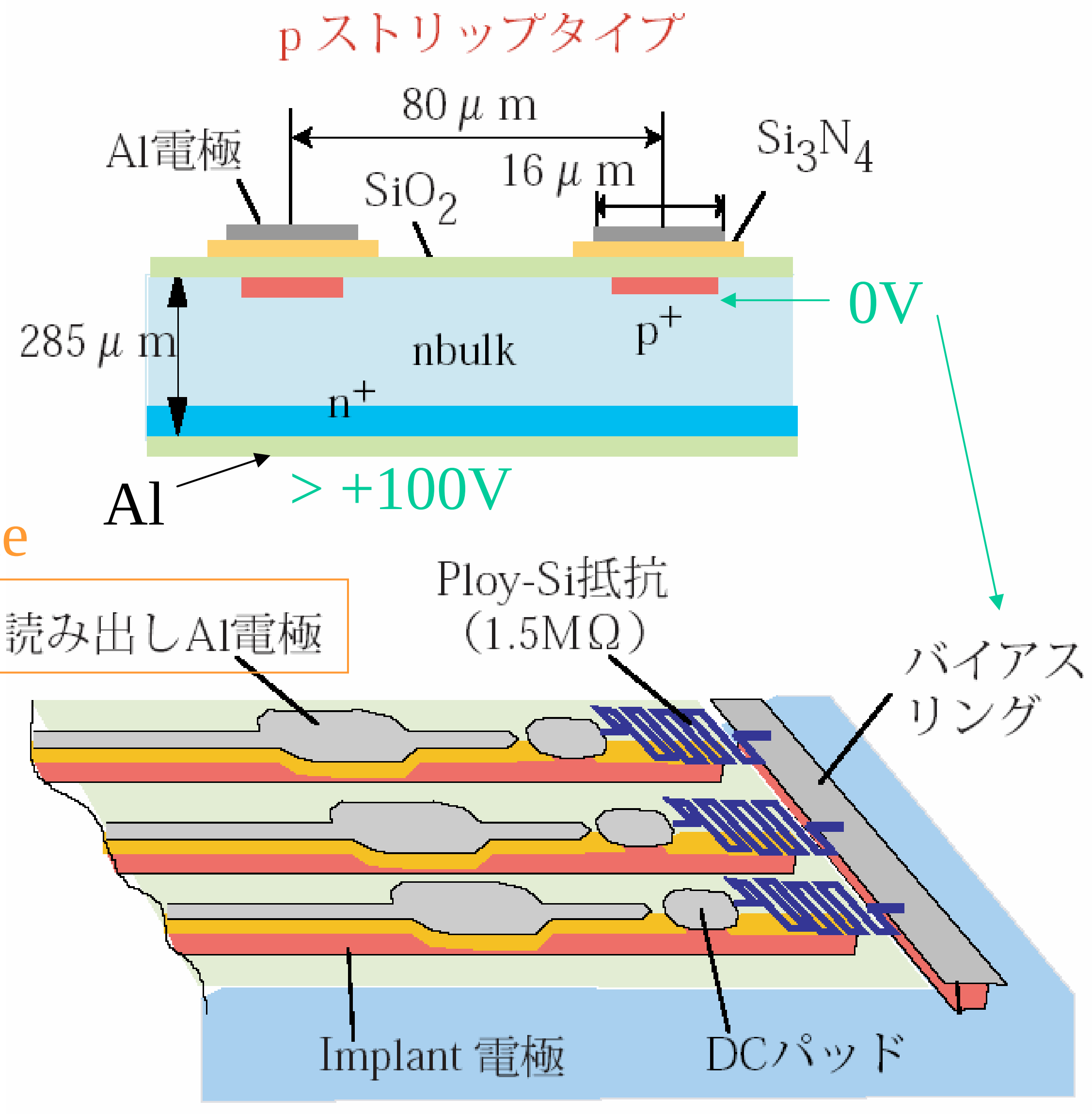

AC couple

SCTの読み出し回路

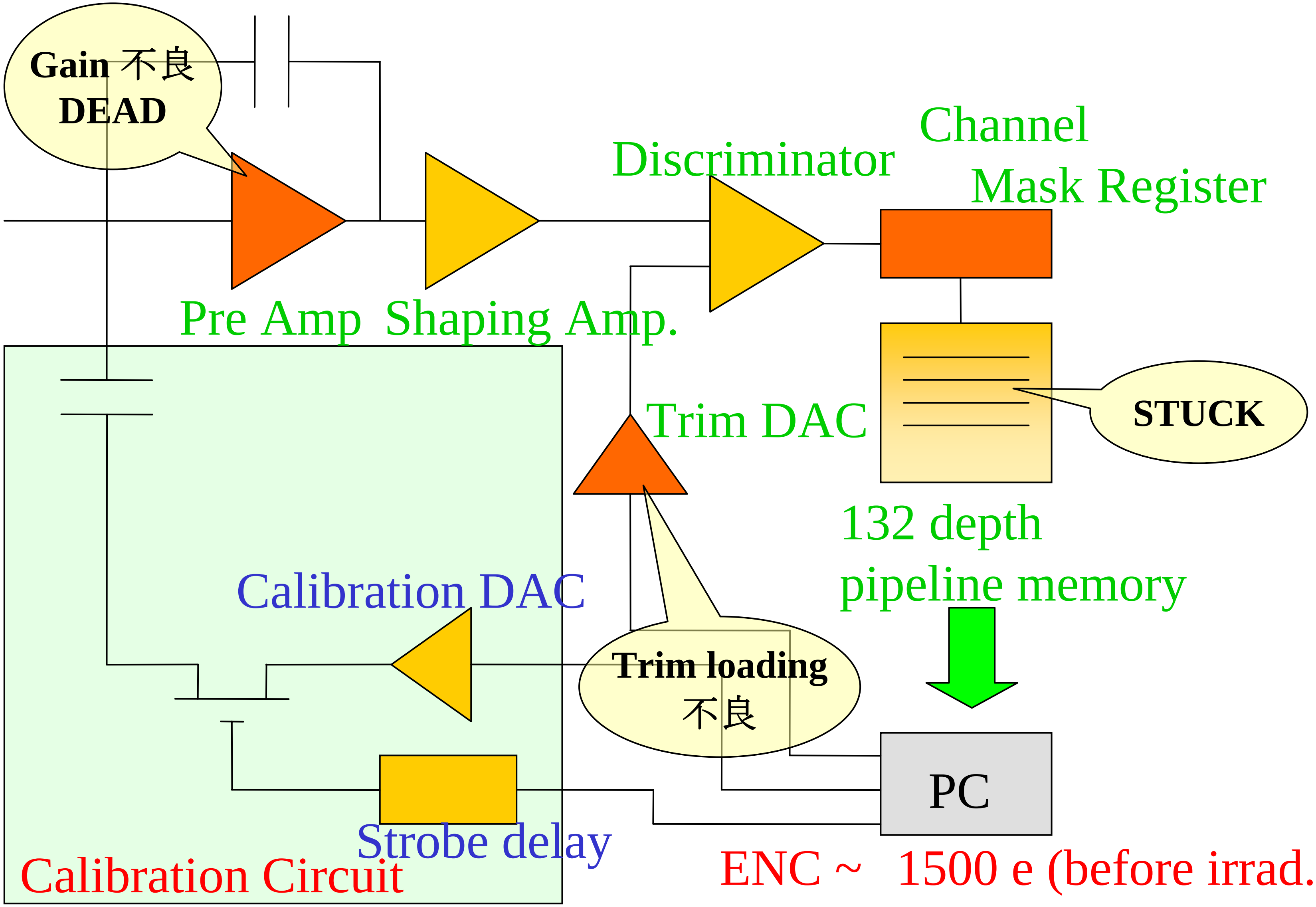

ENC ~ 1500 e (before irrad.)
1800 e (after irrad.)

SCTの特徴 (大面積)

Experiments using silicon strip detectors

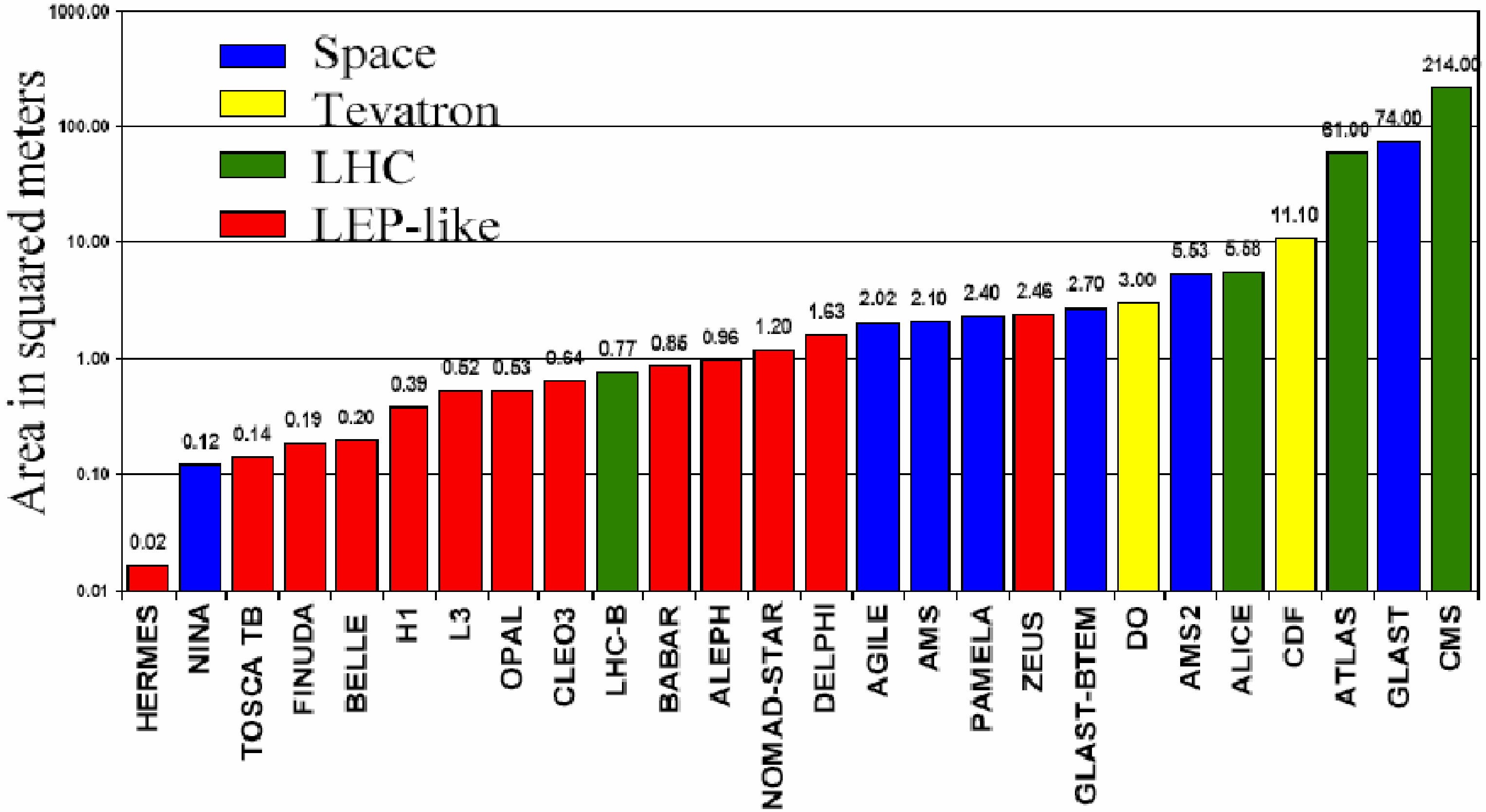

E. do Couto e Silva – SLAC/Stanford University   Vertex 2000, Sept 10-15, National Lakeshore, MI, USA

GSI - 15/11/2002   P.Riedler - CERN

SCTの特徴 (放射線耐性)

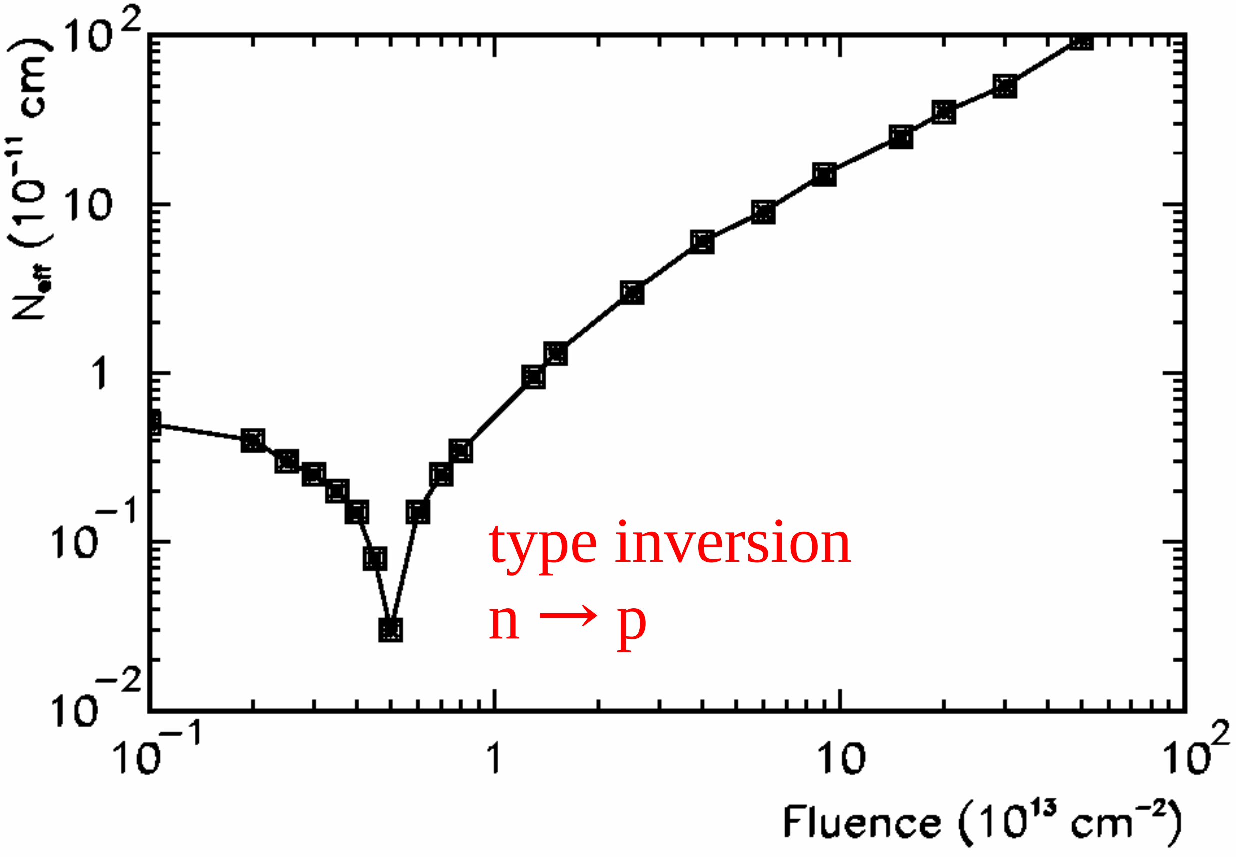

図 2.2: 放射線損傷によるバルク中の有効不純物濃度の変化 [9]

N → 増大
d → 減少
signal → 減少
V (一定)

V → 増大
signal (一定)
d (一定)

収集される電荷量の減少
新たなenergy bandの発生
→キャリヤの捕獲
移動度の低下

暗電流の増加
→ 温度上昇
→ 熱暴走
→ -10℃

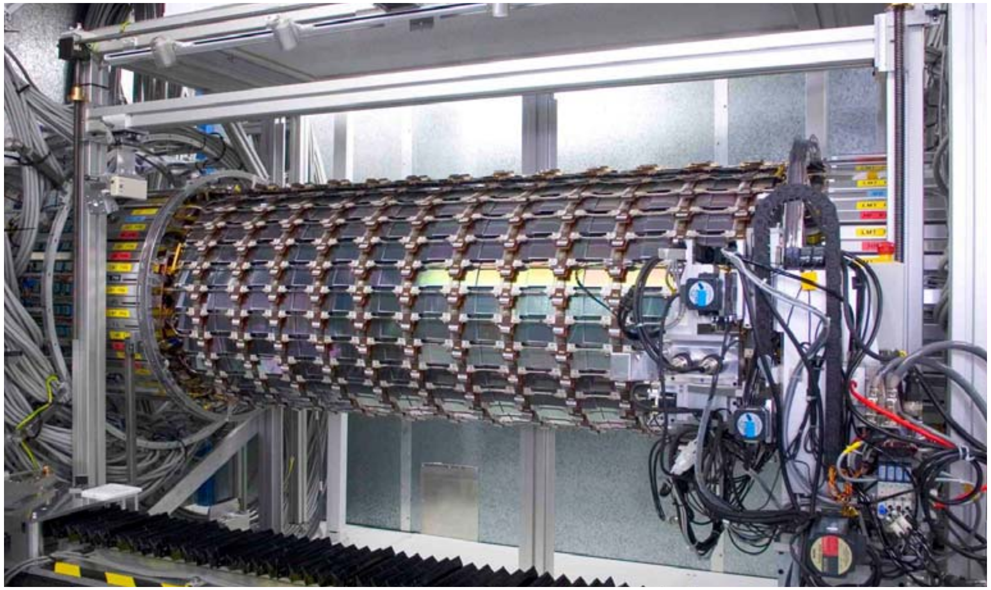

Barrel SCT

2600台のモジュールは全て完成。
B3 : アセンブリー完成しCERNに。
B4 : RALで準備中
B5 : Oxford大で準備中
B6 : Oxford大でマウント中

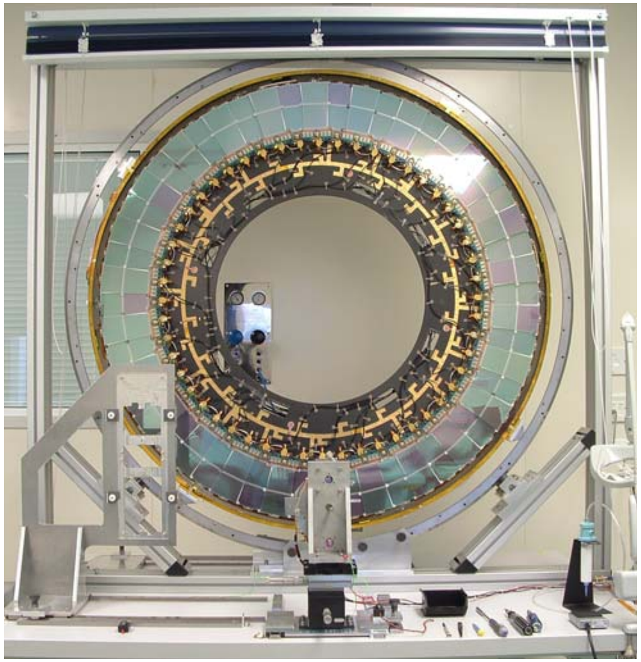

Endcap SCT

73% のモジュールを製造中。

EC(C)
D8,D9 : Liverpool大で完成。
シリンダーに据付られた。
D7,D6 : Liverpool大で準備中。
EC (A) : NIKHEF 5ヶ月遅れ.
9disks x 2

Pixel

The ATLAS-Pixel-Detector

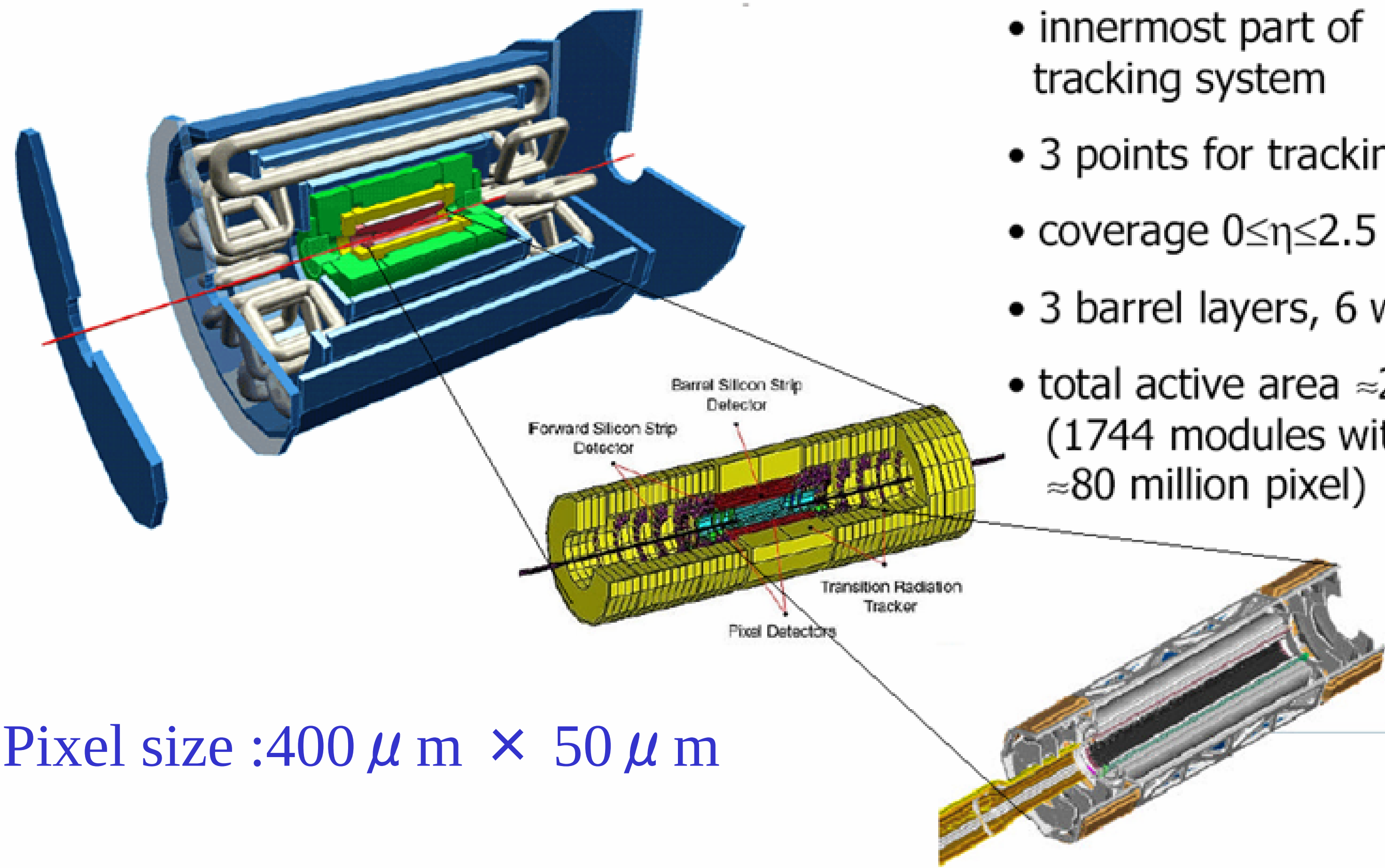

- innermost part of tracking system
- 3 points for tracking
- coverage $0 \leq \eta \leq 2.5$
- 3 barrel layers, 6 wheels
- total active area $\approx 2m^2$ (1744 modules with $\approx$80 million pixel)

Pixel size :400 μ m × 50 μ m

Pixel

Pixel Modules

- Modules are the basic building elements of the detector.
- Each module has an active area of 16.4 mm x 60.8 mm. Each pixel has a 400μm x 50μm area.
- The sensitive area is read out by 16 FE chips which are controlled by a Module Controller Chip (MCC). It decodes data/cmd signals, generate control signal for 16 FEs, collects data from FEs and accumulate in FIFOs, checks event consistency, builds module event and sends to DAQ, handles errors.
- Each FE read-outs 2880 channels organized in a matrix of 18x160 channels. It amplifies sensor signal, on-chip data buffering in EOC FIFOs until trigger signal arrives, sends data on serial link to MCC. On-detector chips are fabricated in 0.25μm DSM by IBM. Used cell library with special layout rules for radiation tolerance.

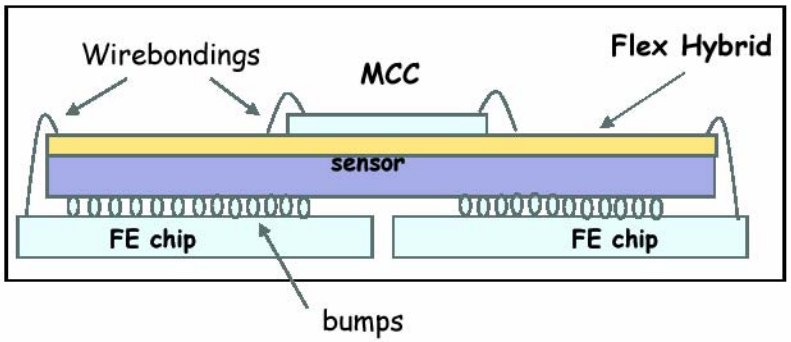

Schematic cross section (through here)

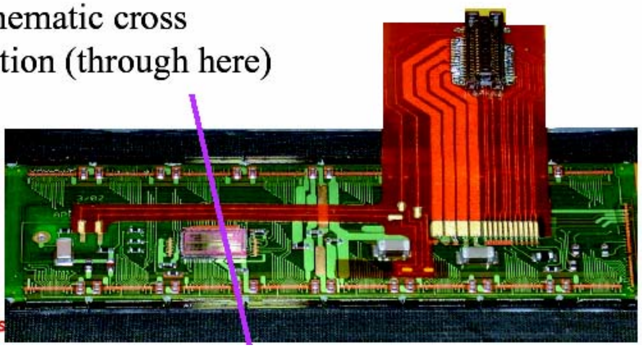

C.Gemme - ATLAS Pixel Modules

Pixel

Detector Concept: p^+-on-n vs. n^+-on-n

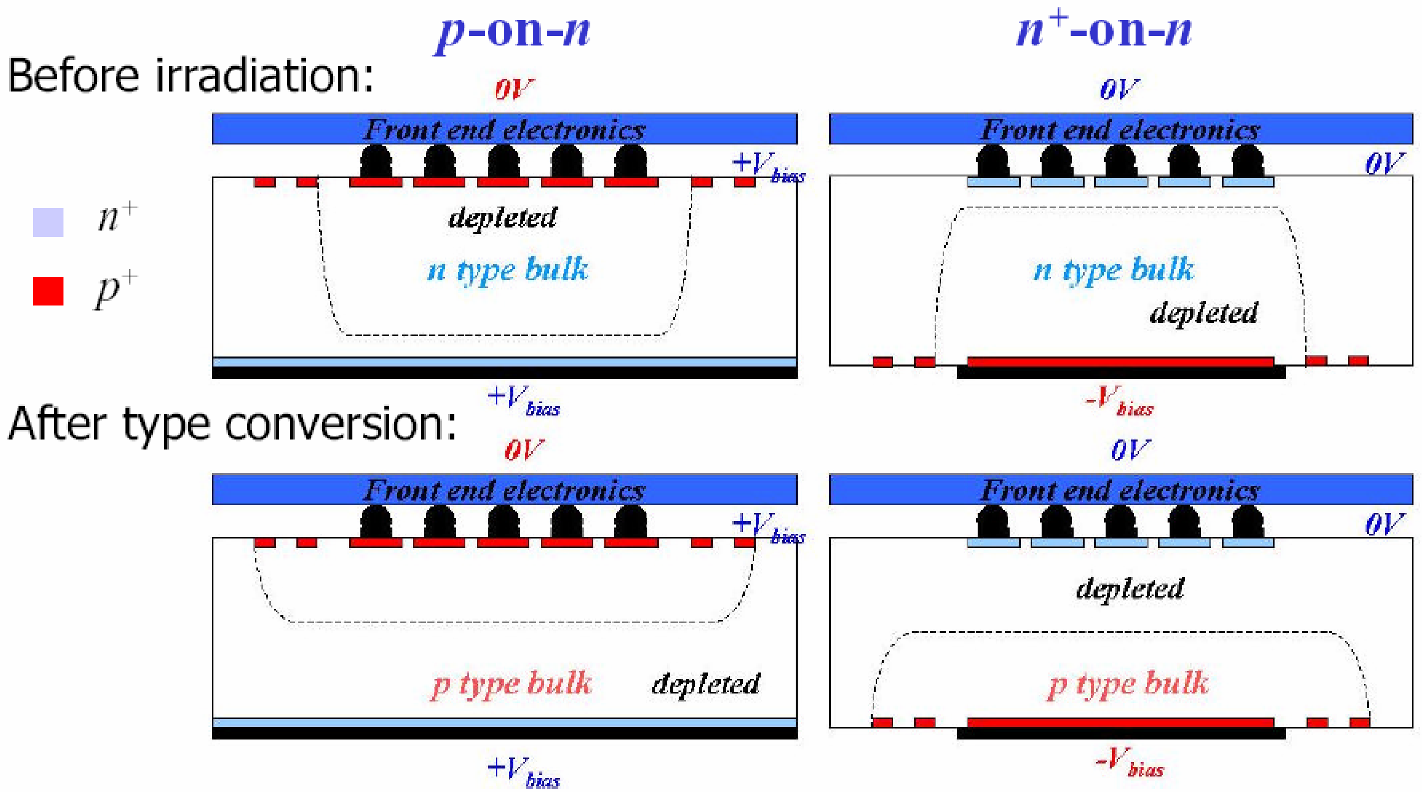

- have to be (almost) fully depleted
- potential drop on the read out side
- only single sided processing necessary

- can be operated partially depleted
- potential drop on the back side
- double sided processing needed

Pixel

Pixel Isolation: Design Options

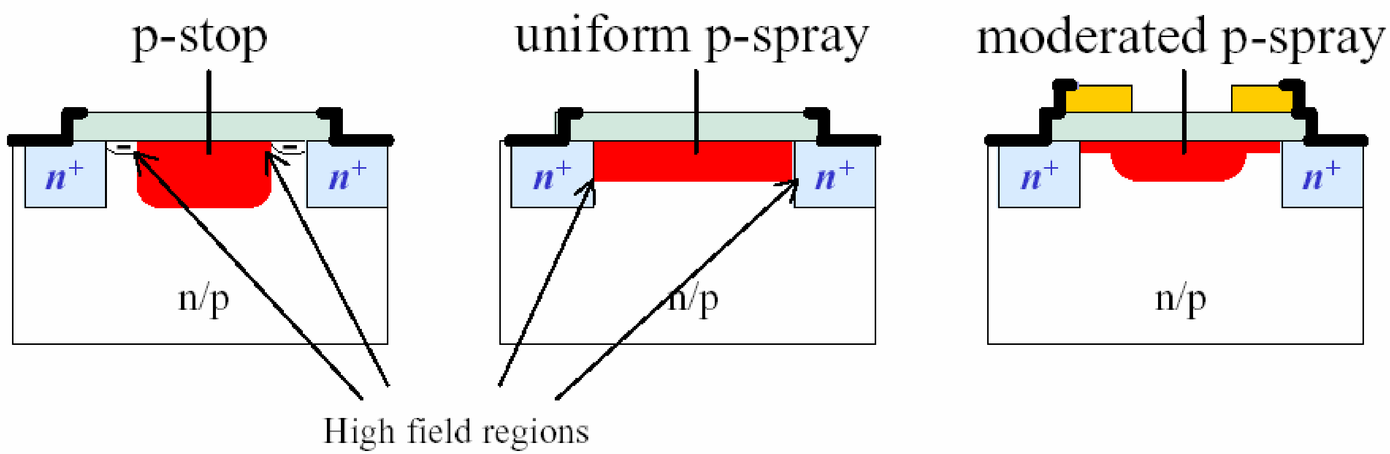

Before irrad.:	low E-field ⇒ high breakdown voltage	high E-field ⇒ low breakdown voltage	low E-field ⇒ high breakdown voltage
After irrad.:	high E-field ⇒ low breakdown voltage	low E-field ⇒ high breakdown voltage	low E-field ⇒ high breakdown voltage
under irradiation:	degrades	improves	improves

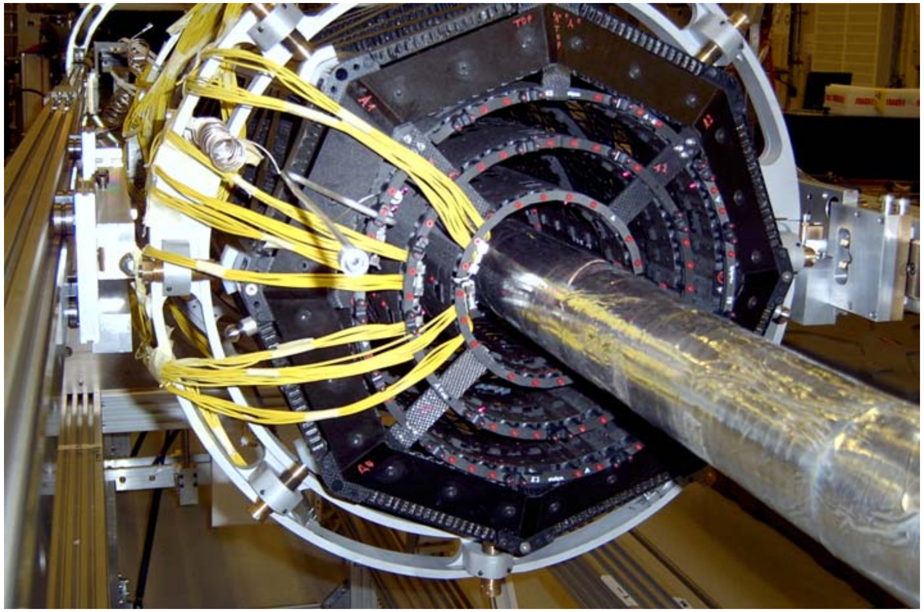

Stave Pixel

- フレームは完成。
- 600モジュール完成
  （3 layer：2100モジュール必要）
- 3 layerは出来そうだ。

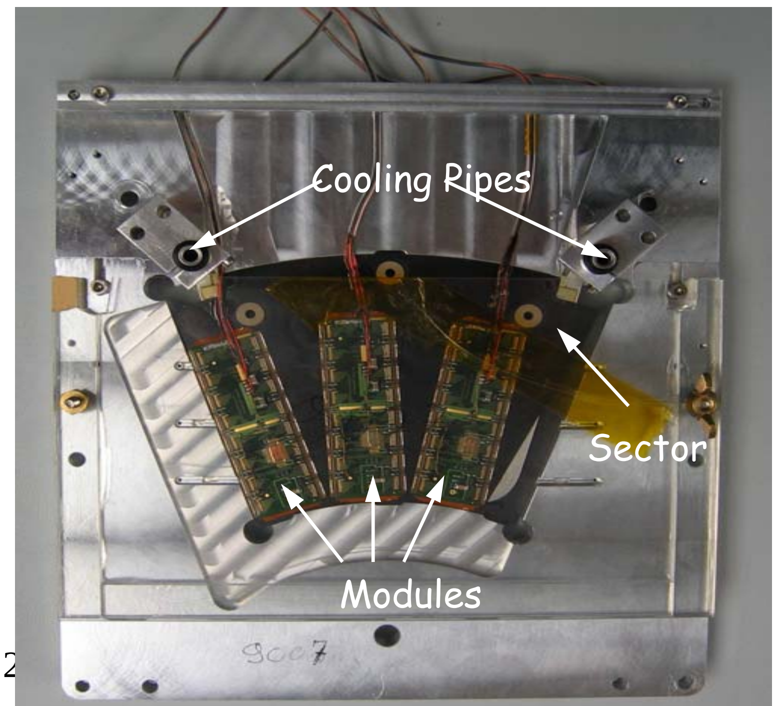

Disk Pixel

12 Sector完成

48 sectors → 11/3/2006

CMSとの比較

2 general purpose detectors:

Higgs in SM and in MSSM, supersymmetric Particles, B physics (CP violation, ...),...

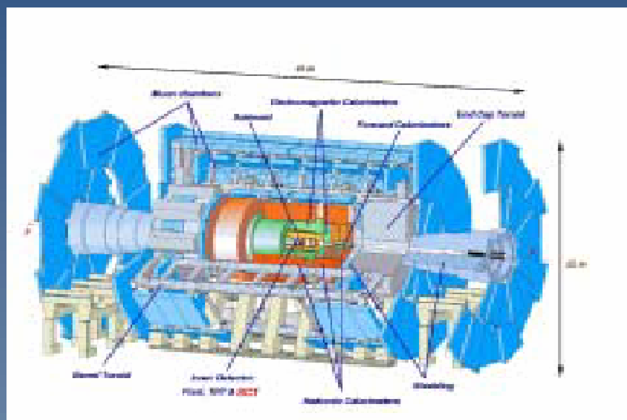

ATLAS

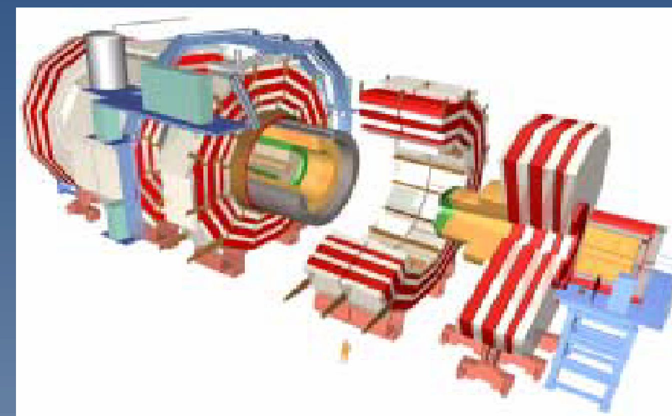

CMS

	ATLAS	CMS
Strips:	$61m^2$, 6.3×10^6 channels	$210m^2$, 9.6×10^6 channels
Pixels:	$\sim 2m^2$, 80×10^6 channels	$\sim 2m^2$, 33×10^6 channels

GSI - 15/11/2002 *P.Riedler - CERN* *7*

CMSとの比較

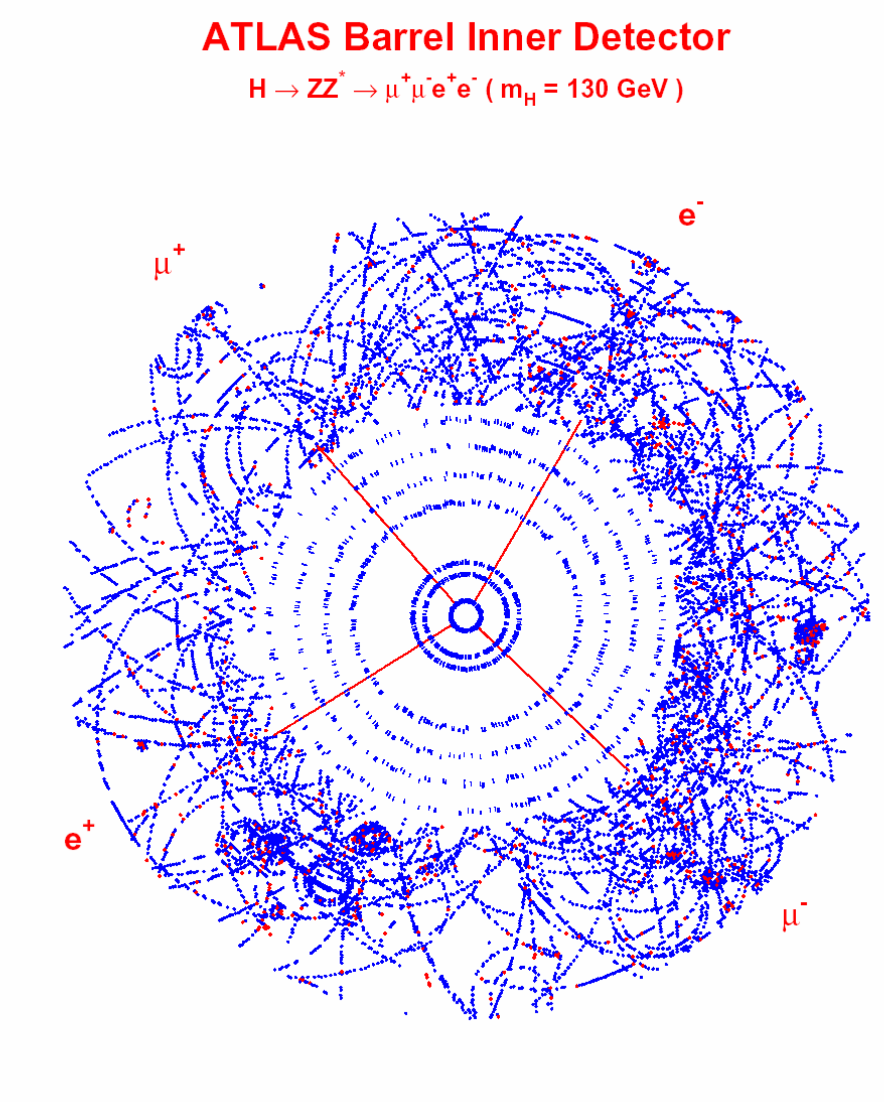

Figure 1-ii Event display of the process $H \to ZZ^* \to \mu^+\mu^-e^+e^-$ in the barrel part of the Inner Detector.

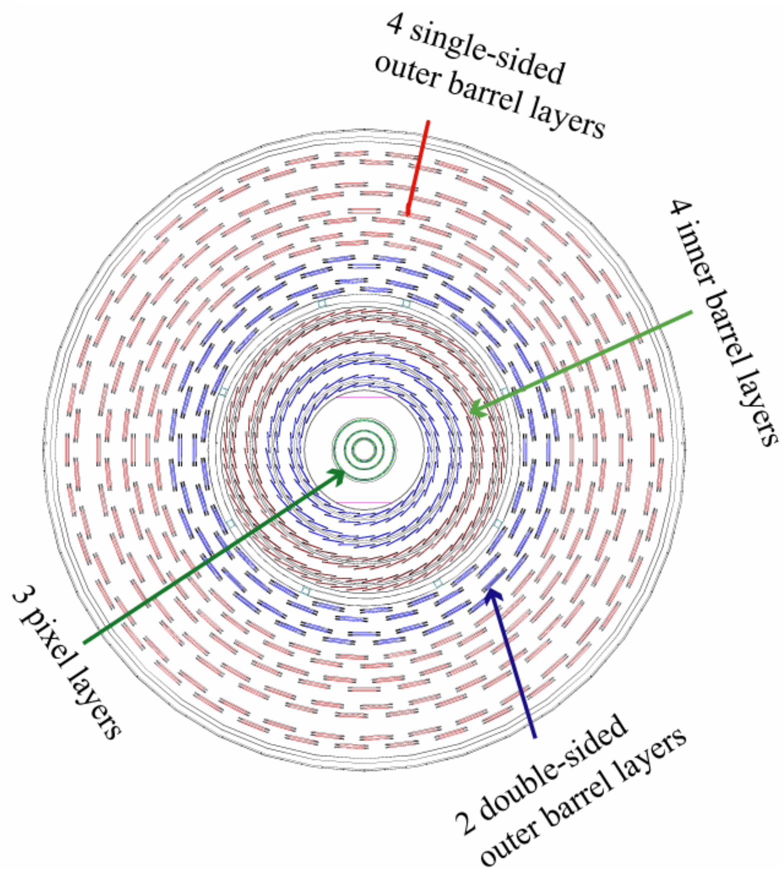

CMSとの比較

Choice of LHC experiments:

ALICE pixel	p-in-n	standard FZ	
ATLAS pixel	n-in-n	oxygenated	
ATLAS strips	p-in-n	standard FZ	
CMS pixel	n-in-n	standard FZ	
CMS strips	p-in-n	standard FZ	<100>
LHCb VELO	n-in-n	standard FZ	

GSI - 15/11/2002 *P.Riedler - CERN* *26*

Wafer 製造法

CZ法：Siをルツボに入れて融かし，不純物を添加する．ピアノ線で吊したSi種結晶を接触させ，シードを回転させながら徐々に引き上げていくと，種結晶に従って単結晶が成長する．最近では，Si単結晶中の酸素濃度を抑えるMCZ法（Magnetic　CZ法）が，ウェーハの大口径化とも関連して採用されつつある．集積回路の製造にはCZ−Si単結晶が広く用いられている．

FZ法：棒状の多結晶Siを吊し，高周波コイルで加熱して部分的に帯状に溶かす．融液部分に小さな種結晶を接触させてから，帯状の溶解部分を上方に移動させ，全体を徐々に単結晶化させる．FZ法では，ルツボを用いないため酸素含有量を少なくできるが，ウェーハの大口径化が困難である．

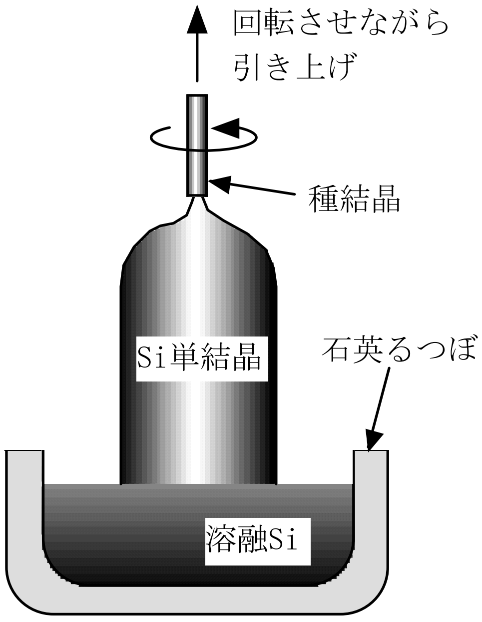

(a) CZ法の概念図

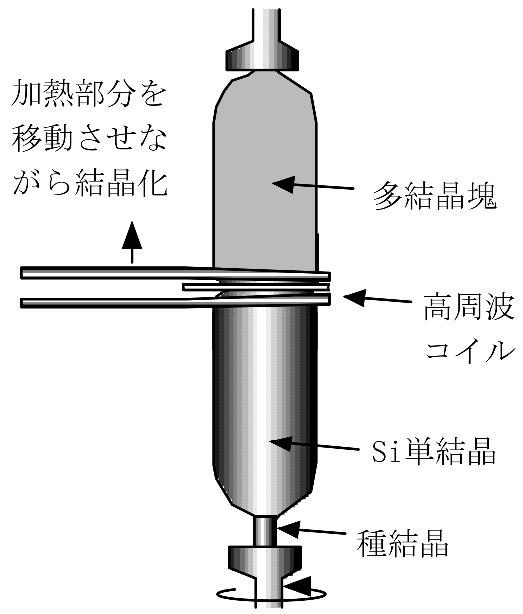

(b) FZ法の概念図

図7-4　単結晶シリコンインゴットの製造方法

Standard track quality cuts

- Number of precision hits ≥ 9 (out of a maximum of ~11, ignoring overlaps).
- Number of pixel hits ≥ 2 (out of a maximum of 3, ignoring overlaps).
- At least one associated hit in the *B*-layer.
- Transverse impact parameter < 1 mm.

pixel & SCT

- Number of TRT straw hits ≥ 20.

out of 36 average hits

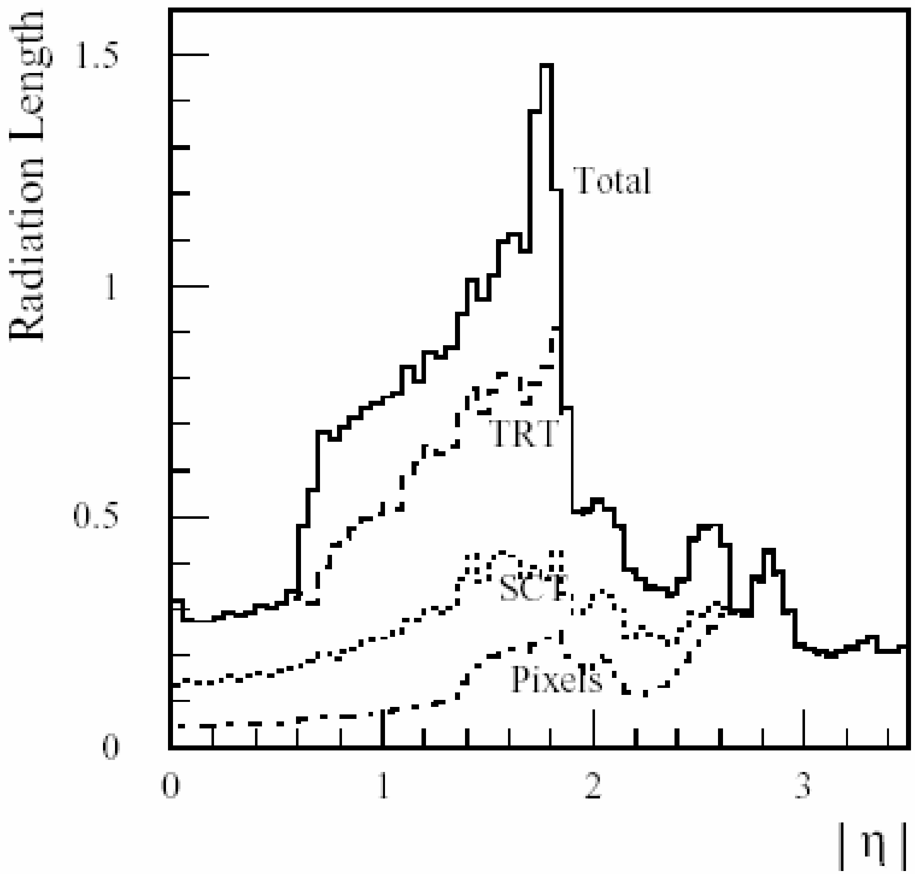

Figure 3-5 Material distribution of the ID vs |η| for the 98_2 layout, used in this report. The various bands include all services and supports within the corresponding fiducial volumes. The pixel band also includes the beam pipe. The total includes the ID services outside the TRT.

muon

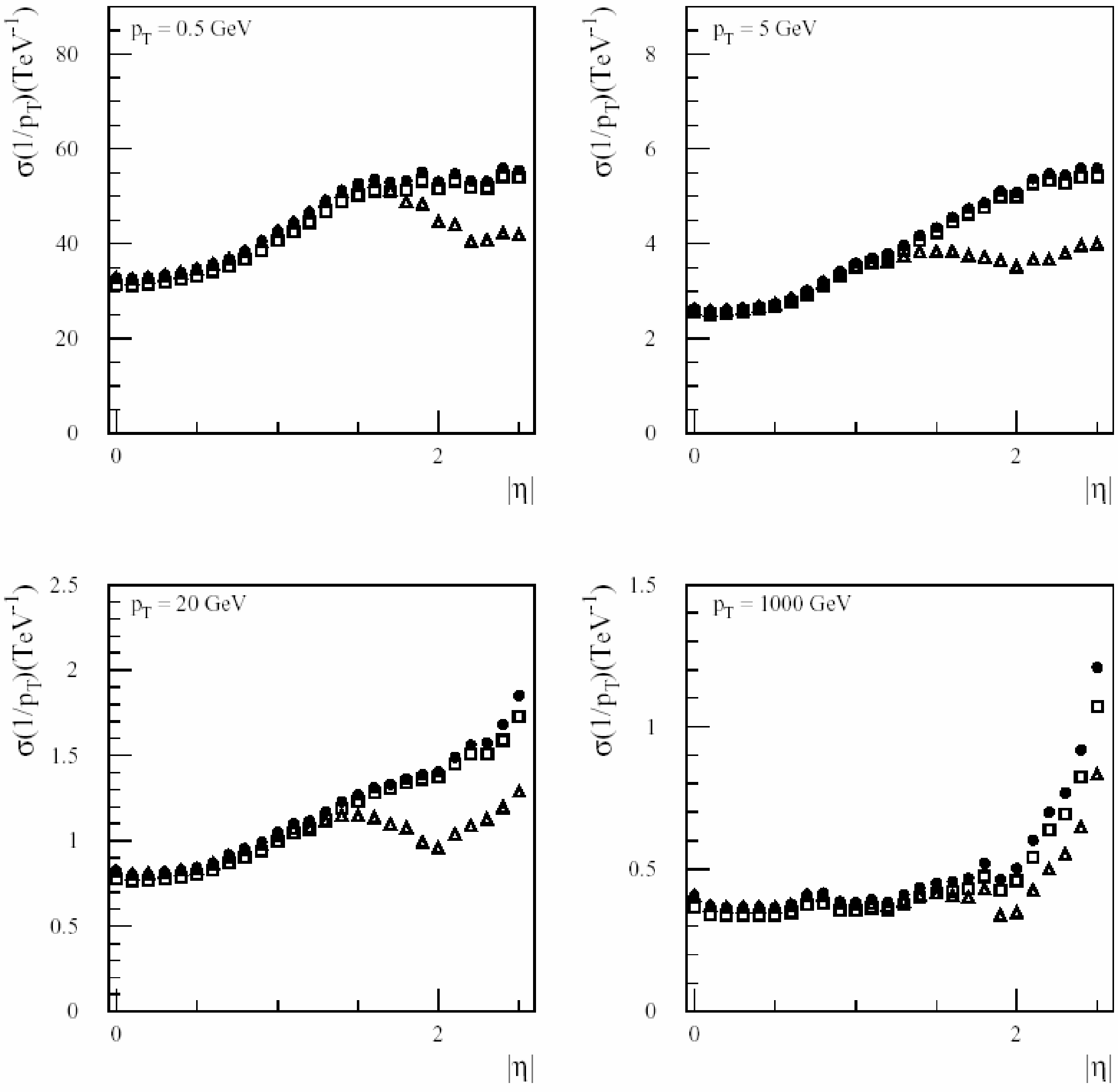

$\sigma p/P = P(TeV)\,\sigma(1/p)$

Figure 3-8 p_T resolution as a function of $|\eta|$ for muons of various momenta. Results are shown for a solenoidal field without (circles) and with (squares) a beam constraint, and for a uniform field without a beam constraint (triangles).

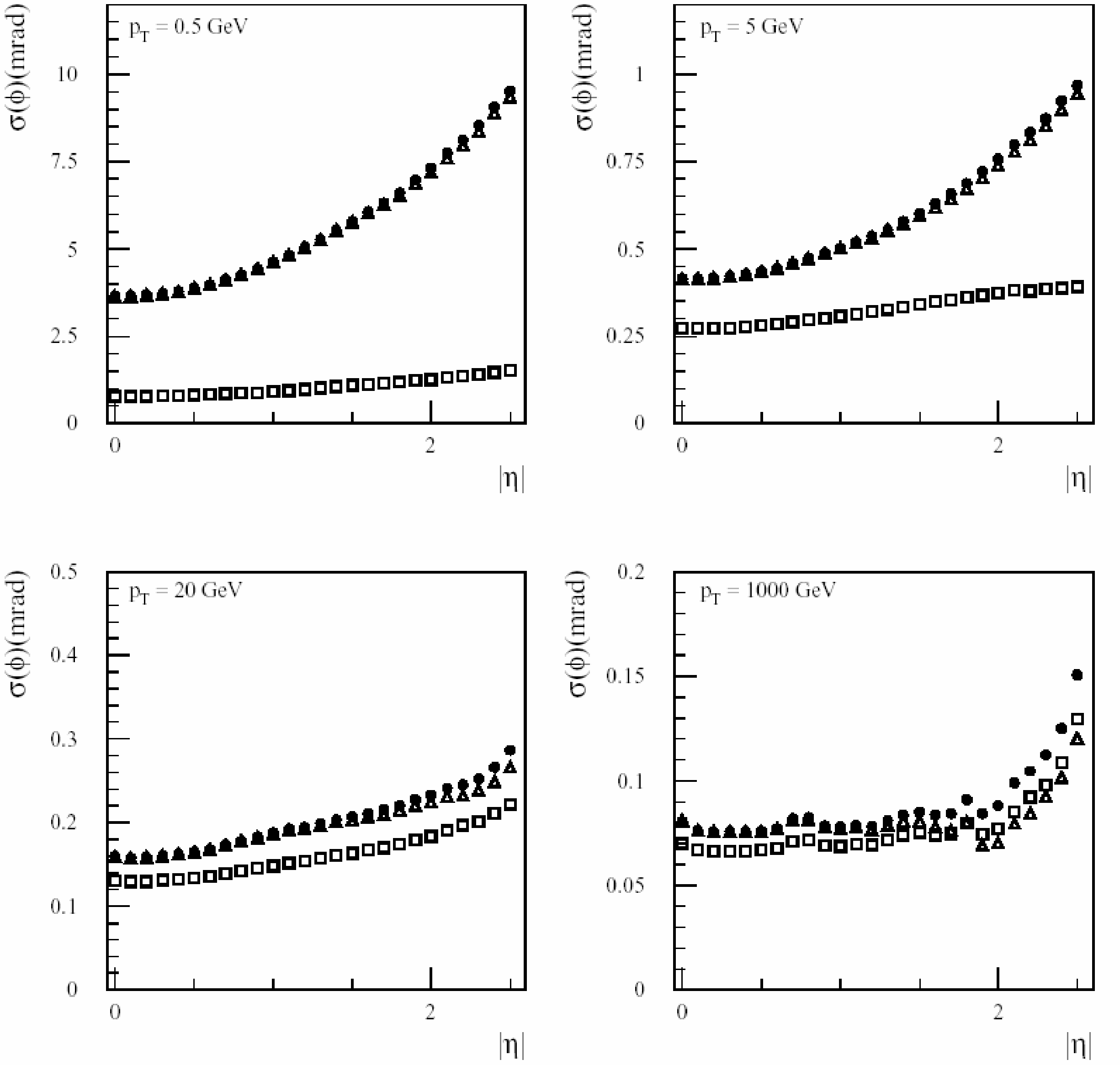

Figure 3-9 Azimuthal resolution as a function of |η| for muons of various momenta. Results are shown for a solenoidal field without (circles) and with (squares) a beam constraint, and for a uniform field without a beam constraint (triangles).

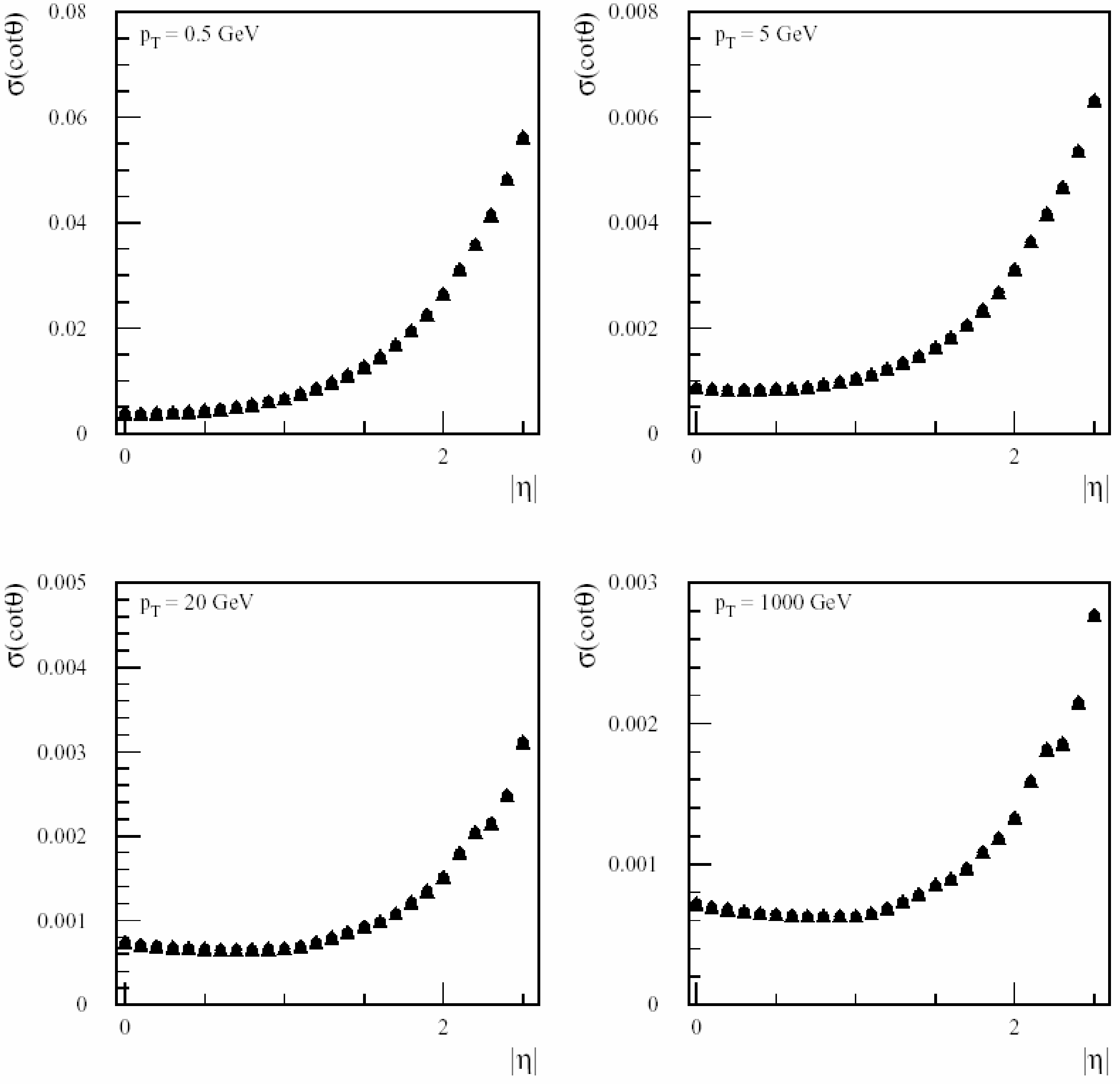

Figure 3-10 cot θ resolution as a function of |η| for muons of various momenta. Results are shown for a solenoidal field (circles) and for a uniform field (triangles) without a beam constraint.

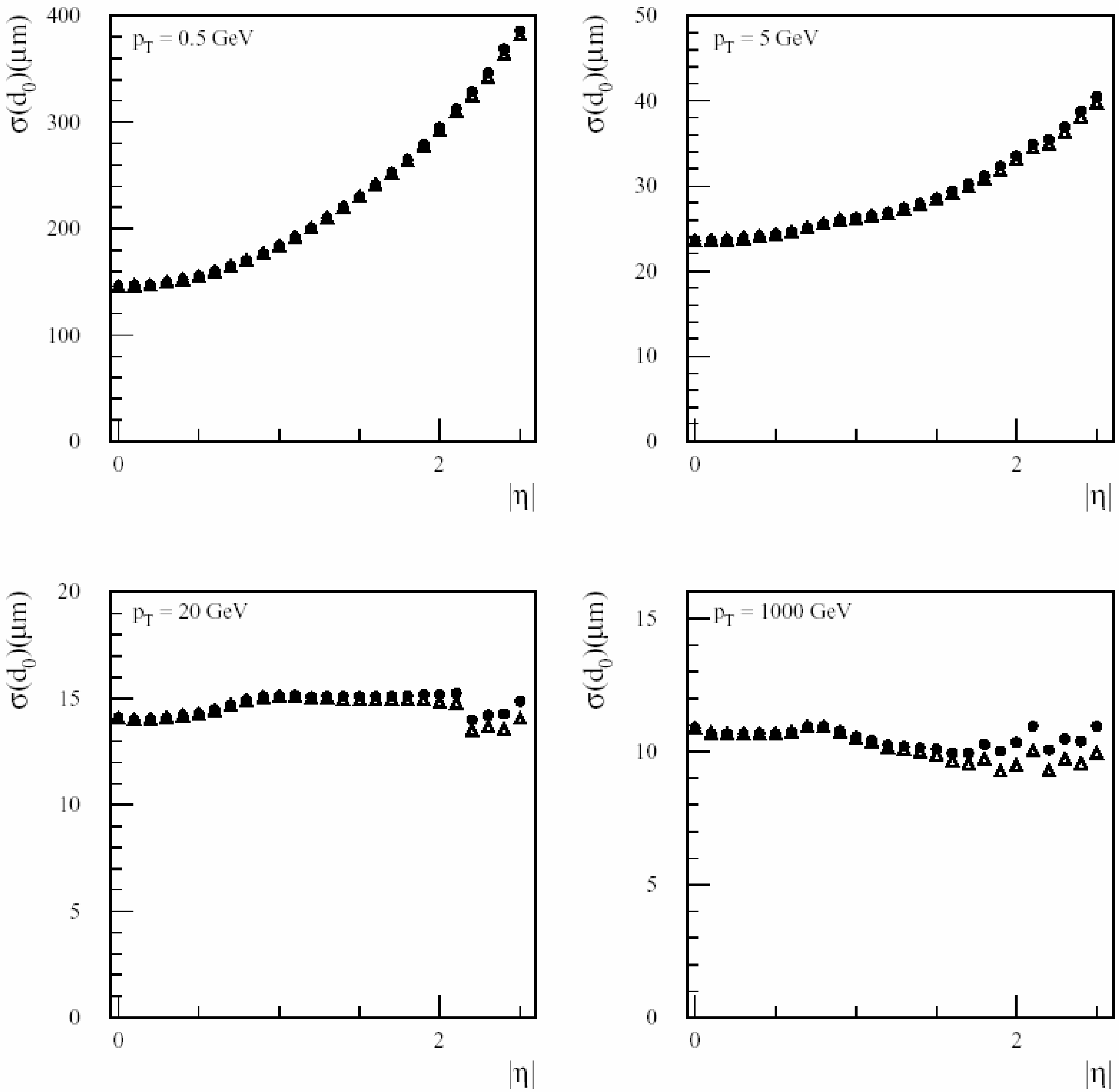

Figure 3-11 Transverse impact parameter (d_0) resolution as function of $|\eta|$ for muons of various momenta. Results are shown for a solenoidal field (circles) and for a uniform field (triangles) without a beam constraint.

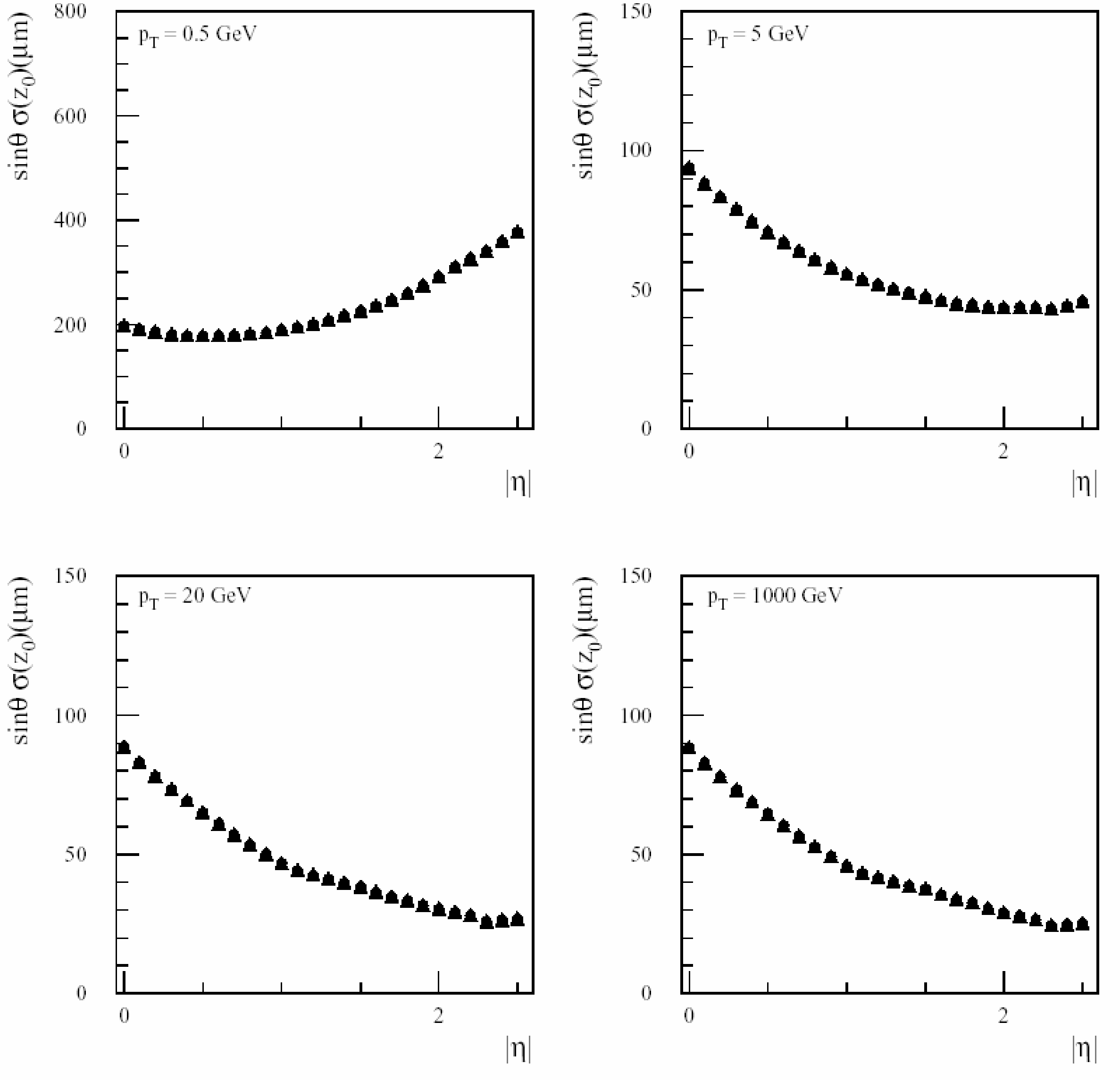

Figure 3-12 Longitudinal impact parameter (z_0) resolution projected transversely to the track direction as function of |η| for muons of various momenta. Results are shown for a solenoidal field (circles) and for a uniform field (triangles) without a beam constraint.

$$\sigma\left(\frac{1}{p_T}\right) \approx 0.36 \oplus \frac{13}{p_T\sqrt{\sin\theta}} \qquad (\mathrm{TeV}^{-1})$$

GeV

$$\sigma(\phi) \approx 0.075 \oplus \frac{1.8}{p_T\sqrt{\sin\theta}} \qquad (\mathrm{mrad})$$

$$\sigma(\cot\theta) \approx 0.70 \times 10^{-3} \oplus \frac{2.0 \times 10^{-3}}{p_T\sqrt{\sin^3\theta}}$$

$$\sigma(d_0) \approx 11 \oplus \frac{73}{p_T\sqrt{\sin\theta}} \qquad (\mu\mathrm{m})$$

$$\sigma(z_0) \approx 87 \oplus \frac{115}{p_T\sqrt{\sin^3\theta}} \qquad (\mu\mathrm{m})$$

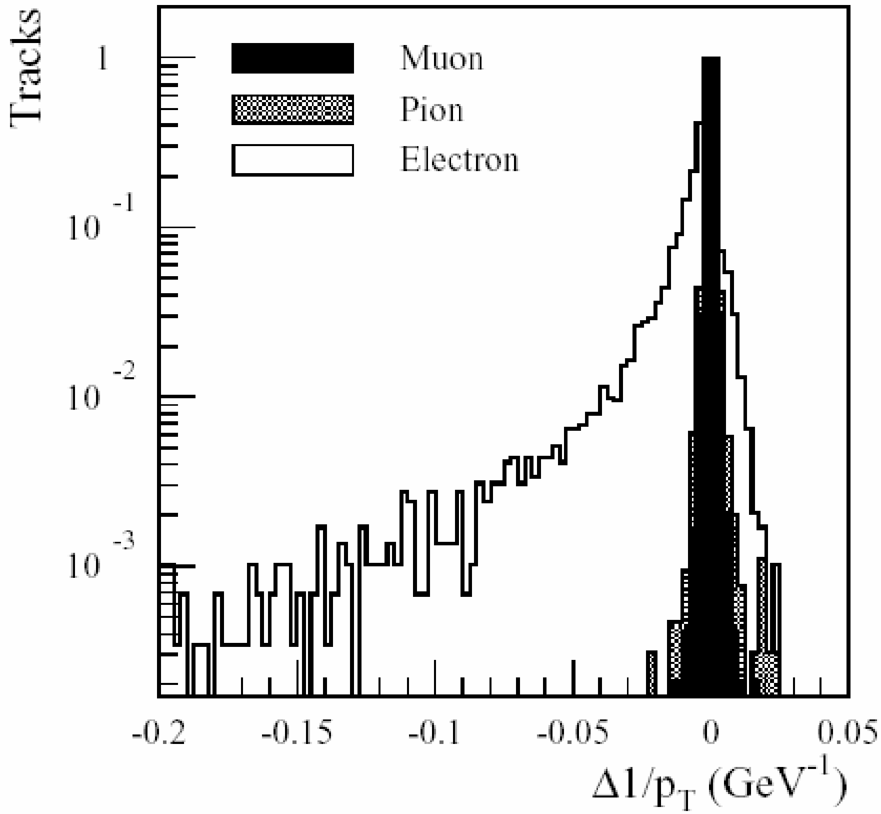

Figure 3-19 Difference between the reconstructed and generated $1/p_T$ for single 20 GeV negatively charged particles.

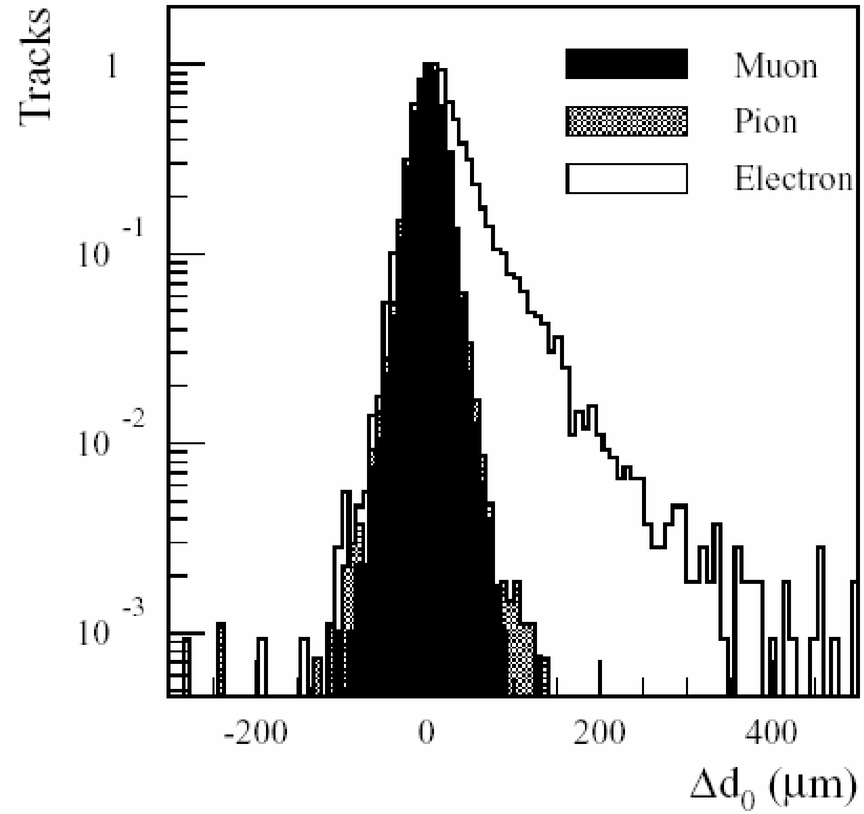

Figure 3-20 Difference between the reconstructed and generated transverse impact parameter for single 20 GeV negatively charged particles.

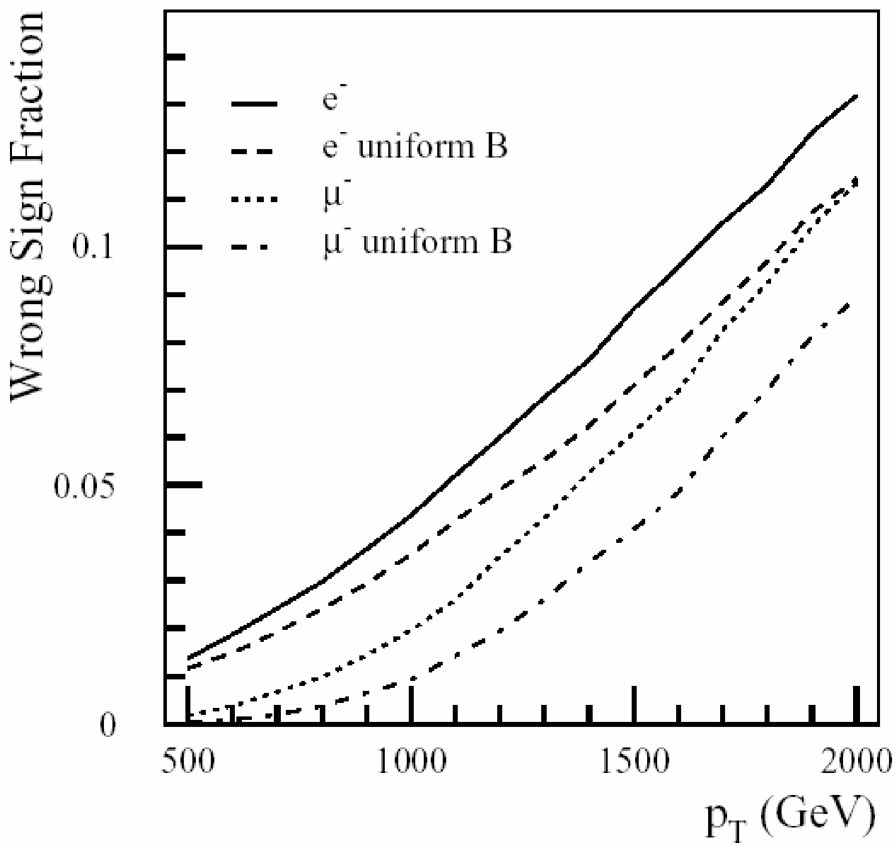

Figure 3-22 Wrong sign fraction as a function of p_T for muons and electrons, averaged over pseudorapidity in the presence of either a solenoidal or uniform magnetic field.

Photon measurement

Around 30% of all photons convert in the material of the ID cavity ($R < 115$ cm). Figure 7-30 shows that around 75% of these conversions occur in the volume ($R < 80$ cm, $|z| < 280$ cm) in which they can be efficiently identified. Depending on the pseudorapidity, the conversion fraction within this volume varies between 15% and 30%. Conversions occurring outside this region are less harmful because the electrons do not bend much in the azimuthal direction before entering the EM Calorimeter, and hence look more like unconverted photons.

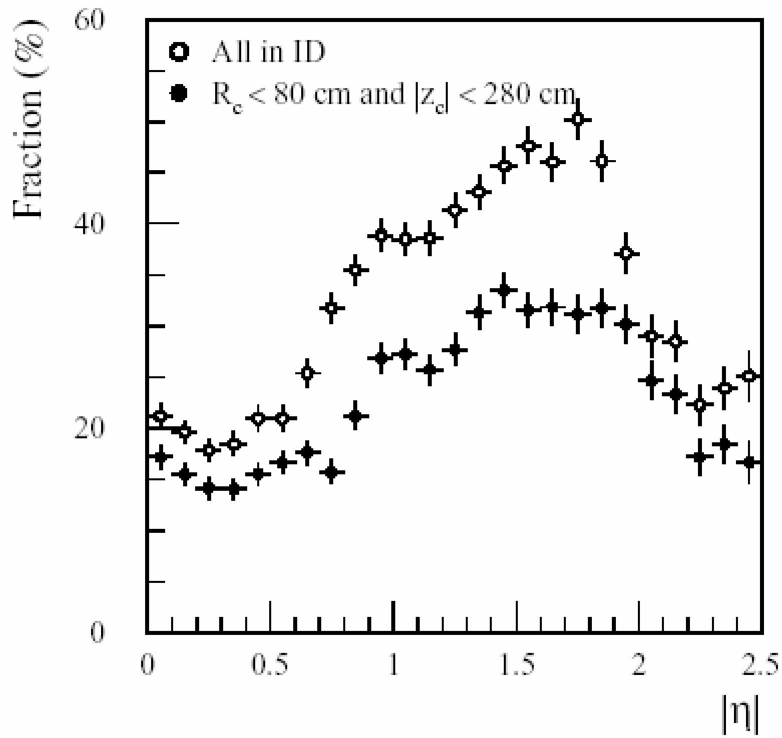

Figure 7-30 Fraction of photons converted in the ID cavity (open symbols) and in the region in which conversions can be efficiently identified (closed symbols) as a function of pseudorapidity.